

This document is confidential and is proprietary to the American Chemical Society and its authors. Do not copy or disclose without written permission. If you have received this item in error, notify the sender and delete all copies.

**Multivalent glycosylation of fluorescent gold nanoclusters promotes increased human dendritic cell targeting via multiple endocytic pathways**

Journal:	<i>ACS Applied Materials &amp; Interfaces</i>
Manuscript ID	am-2015-06541y.R1
Manuscript Type:	Article
Date Submitted by the Author:	28-Aug-2015
Complete List of Authors:	Le Guével, Xavier; The Andalusian Centre for Nanomedicine and Biotechnology (BIONAND), Therapeutic Nanosystems Perrez Perrino, Monica; University of Seville, Glycosystems Laboratory, Instituto de Investigaciones Químicas (IIQ), CSIC Fernández, Tahia; Málaga Regional University Hospital, UMA, Research Laboratory and Allergy Service, IBIMA Pomares, Francisca; Málaga Regional University Hospital, UMA, Research Laboratory and Allergy Service, IBIMA Torres, Maria Jose; Carlos Haya Hospital, Blanca, Miguel; Carlos Haya Hospital, Rojo, Javier; CSIC, Instituto de Investigaciones Químicas Mayorga, Cristobalina; Málaga Regional University Hospital, UMA, Research Laboratory and Allergy Service, IBIMA

SCHOLARONE™  
Manuscripts

1  
2  
3 Multivalent Glycosylation of Fluorescent Gold Nanoclusters promotes increased  
4 Human Dendritic Cell Targeting via Multiple Endocytic Pathways  
5  
6  
7

8 Xavier Le Guével<sup>1\*</sup>, Monica Perrez Perrino<sup>2</sup>, Tahia D Fernández<sup>3</sup>, Francisca Pomares<sup>3</sup>, Maria-  
9 José Torres<sup>4</sup>, Miguel Blanca<sup>4</sup>, Javier Rojo<sup>2</sup>, Cristobalina Mayorga<sup>3,4</sup>  
10  
11

12  
13 <sup>1</sup> Therapeutic Nanosystems, The Andalusian Centre for Nanomedicine and Biotechnology  
14 (BIONAND), Málaga, Spain  
15  
16

17  
18 <sup>2</sup> Glycosystems Laboratory, Instituto de Investigaciones Químicas (IIQ), CSIC – University of  
19 Seville, Spain  
20  
21

22  
23 <sup>3</sup> Research Laboratory and Allergy Service, IBIMA, Málaga Regional University Hospital,  
24 UMA, Málaga, Spain  
25

26  
27 <sup>4</sup> Allergy Service, IBIMA, Regional University Málaga Hospital, UMA, Málaga, Spain  
28

29 \*Address correspondence to  
30

31 xleguevel@bionand.es  
32

33 Tel.: +34 952 367 648  
34

35 Fax: +34 952 367 610  
36  
37  
38  
39  
40  
41

42 **ABSTRACT**

43 We report the synthesis and characterisation of gold nanoclusters (Au NCs) stabilised by a  
44 mixture of zwitterionic and multivalent mannose ligands. Characterisation of this carbohydrate  
45 nanosystem confirms its small size (~2 nm), intense red-NIR fluorescence, relatively high  
46 affinity to lectin (ConA), and stability in physiological media. Cell studies performed using  
47 human monocyte-derived dendritic cells (DCs) show that Au NC uptake efficiency is greatly  
48 enhanced by the presence of surface carbohydrate (> 250% compared to non-carbohydrated Au  
49  
50  
51  
52  
53  
54  
55  
56  
57  
58  
59  
60

1  
2  
3 NCs) allowing their detection in cells by fluorescence following incubation with concentrations  
4  
5 as low as 1  $\mu\text{g}\cdot\text{mL}^{-1}$ . Investigation using electron microscopy and pharmacological inhibitors  
6  
7 indicates that Au NC uptake is mediated by multiple endocytic pathways involving the  
8  
9 engulfment of Au NCs into endosomes and partial transport to lysosomes. Results show that  
10  
11 clathrin and F-actin dependent pathways play major roles in Au NC uptake by DCs regardless of  
12  
13 whether or not they are coated with carbohydrates. In contrast, a specific C-lectin inhibitor  
14  
15 induces a 60% decrease in DC particle uptake only for the carbohydrate-coated Au NCs. This  
16  
17 study demonstrates that the combination of ultra-small gold NCs and functionalisation with  
18  
19 multivalent mannose ligands results in greatly enhanced human DC targeting, presumably due to  
20  
21 increased diffusion and target cell binding, respectively.  
22  
23  
24  
25  
26  
27

28 **KEYWORDS:** gold nanoclusters, mannose, targeting, cell uptake, dendritic cells  
29  
30  
31  
32

## 33 INTRODUCTION

34  
35

36 As part of the development of nanoparticle (NP)-vaccines for the treatment of cancer,  
37  
38 infectious diseases and allergies, many efforts have focused on dendritic cell (DC)  
39  
40 targeting<sup>1-3</sup>. DCs are one of the most potent types of antigen presenting cell (APC) and  
41  
42 are seen as key players in the initiation and control of adaptive immune responses<sup>4-5</sup>.  
43  
44 Furthermore, DCs reside in the periphery and in lymphoid organs, which make them ideal  
45  
46 sentinels for pathogen recognition. As a consequence, a new generation of particulate-  
47  
48 based vaccines are designed to i) target DCs in specific tissues, and ii) efficiently deliver  
49  
50 antigens to DCs to either stimulate the immune response for immunotherapy or  
51  
52 downregulate it for the treatment of allergic diseases or organ transplantation<sup>6-8</sup>.  
53  
54  
55  
56  
57  
58  
59  
60

1  
2  
3 One of the main potential advantages of using NPs for vaccines is based on their capacity  
4 to stabilise vaccine antigens while simultaneously acting as an adjuvant<sup>6, 9-10</sup>. Antigens  
5  
6 can be encapsulated or conjugated to the NP surface, with both methods offering distinct  
7  
8 advantages. For instance, the loading of allergens inside NPs is an elegant strategy to  
9  
10 protect the therapeutic agent from clearance at the injection site<sup>11</sup>, while surface  
11  
12 conjugation enhances immune cell antigen presentation<sup>12</sup>. In addition, NPs are attractive  
13  
14 for clinical and biological applications due to their low immunogenicity, low toxicity, and  
15  
16 good biocompatibility<sup>9</sup>. In other words, NPs have the potential, at least in theory, to  
17  
18 deliver antigens efficiently to DCs by different pathways due to our ability to  
19  
20 functionalise their surface with biomolecules and their capacity to modulate the immune  
21  
22 response. Extensive research has focused on a plethora of biodegradable (PLGA,  
23  
24 dendrimers, chitosan, virus-like-particles, liposomes)<sup>1, 13-15</sup> and non-degradable (gold,  
25  
26 silicon, polystyrene)<sup>16-18</sup> NPs designed to reach DCs in in vitro and in vivo models. Two  
27  
28 major NP parameters are considered crucial for efficient DC targeting: 1) NP size, and 2)  
29  
30 NP surface functionalisation. Size has been shown to drastically influence particle  
31  
32 recognition by the immune system where particles bigger than 1  $\mu\text{m}$  are rapidly  
33  
34 phagocytised by macrophages<sup>6</sup>. Studies performed in in vivo models have demonstrated  
35  
36 that NPs enter lymphatic capillaries and are taken up by peripheral DCs close to the  
37  
38 injection site with higher uptake efficiency for particles in the range of 20-200 nm<sup>11, 19</sup>.  
39  
40 Therefore, smaller NPs might reach a higher number of DCs due to their greater diffusion  
41  
42 and penetration. However, determining the relative effectiveness of narrower NP size  
43  
44 ranges has been the subject of contradictory results in in vitro and in vivo models,  
45  
46 revealing the complexity of the different factors involved in NP uptake<sup>20</sup>. Numerous  
47  
48  
49  
50  
51  
52  
53  
54  
55  
56  
57  
58  
59  
60

1  
2  
3 independent studies have shown that the physico-chemical parameters of NPs have a  
4 direct impact on passive DC targeting<sup>18, 21</sup> while the presence of functional surface  
5 groups, such as carbohydrates or antibodies, have been shown to specifically bind DC  
6 surface receptors<sup>22</sup>. This strategy has been remarkably successful, notably by targeting C-  
7 lectin receptors (CLRs) using customised carbohydrate ligands. The mannose receptor  
8 (MR) and DC SIGN are the most important and best characterised CLRs present on the  
9 surface of DCs<sup>23</sup>. Carbohydrate synthesis, the DC targeting efficiency of carbohydrate-  
10 coated NPs and their biological applications have been covered by several excellent  
11 reviews<sup>2, 24</sup>. One elegant approach to enhance CLR targeting involves taking advantage of  
12 the multivalency of carbohydrate compounds. For example, Rojo et al. designed different  
13 glycosystems based on the attachment of multivalent mannoses or fucoses to nanocarriers  
14 (dendrimers<sup>25</sup>, fullerenes<sup>26</sup>) and demonstrated their high uptake efficiency by targeting  
15 DC-SIGN receptors. They also showed how these multivalent “glyconanosystems” could  
16 be applied to inhibit viral infections such as HIV<sup>27</sup> and the Ebola virus with very high  
17 efficiency and selectivity<sup>26, 28-29</sup>.

18  
19  
20  
21  
22  
23  
24  
25  
26  
27  
28  
29  
30  
31  
32  
33  
34  
35  
36  
37  
38  
39  
40  
41 Metal (Au, Ag, Pt, Cu) nanoclusters (NCs) are a family of particles composed from  
42 just a handful of atoms up to ~100 atoms, thus spanning the gap between individual atom  
43 and nanoparticle properties. NCs exhibit unique optoelectronic properties due to their  
44 strong quantum confinement in this size regime (~0.5 nm for Au and Ag)<sup>30-31</sup>. Recently,  
45 numerous Au and Ag NCs have been reported that exhibit intense luminescence in a  
46 broad spectral range stretching from UV to near infrared (NIR)<sup>31</sup>. Such nanostructures  
47 require stabilising agents, or templates, to maintain their stability in solution and prevent  
48 the loss of their unique optical properties. Commonly reported templates for Au and Ag  
49  
50  
51  
52  
53  
54  
55  
56  
57  
58  
59  
60

1  
2  
3 NCs include dendrimers<sup>32</sup>, biomolecules (DNA, proteins, peptides, etc.)<sup>33</sup> and thiolated  
4 molecules<sup>34</sup>. In the latter example, extensive experimental studies supported by  
5 theoretical models<sup>30, 35</sup> demonstrate that both the NC core and the thiolated gold (I) shell  
6 contribute to their photoluminescence properties, with the shell being especially important  
7 for red-NIR region emissions<sup>36-39</sup>. For instance, the Mattoussi lab reported the preparation  
8 of red-emitting Au NCs with a quantum yield of up to 14% when stabilised with bidentate  
9 thiolated ligands containing a zwitterionic group<sup>40</sup>. NC features such as tunable  
10 photoluminescence<sup>41-42</sup>, multiexponential fluorescence lifetime<sup>43-44</sup>, or aggregation  
11 induced enhancement<sup>45</sup> have been extensively studied with potential applications in the  
12 fields of sensing<sup>46</sup>, bioimaging<sup>47</sup> and optics<sup>48</sup>. Other interesting properties of NCs relevant  
13 for therapeutic applications rely on their ultra-small size, low toxicity and stability in  
14 physiological media. In vitro studies in mice have demonstrated the rapid and efficient  
15 clearance of glutathione stabilised-Au NCs due to their size being smaller than the kidney  
16 filtration threshold ( $\varnothing \sim 5.5 \text{ nm}$ )<sup>49-50</sup>. NCs have shown also promising results for cancer  
17 therapy<sup>49, 51</sup> and vaccine development<sup>52</sup>. For example, we have recently shown how their  
18 small size and the use of a zwitterionic ligand promotes their uptake by monocyte-derived  
19 DCs and induces a strong immunosuppressive effect<sup>52</sup>, which we believe to be related to  
20 the dual action of the high diffusion of the particle in solution and the ligand contribution.  
21  
22  
23  
24  
25  
26  
27  
28  
29  
30  
31  
32  
33  
34  
35  
36  
37  
38  
39  
40  
41  
42  
43  
44  
45  
46  
47  
48  
49  
50  
51  
52  
53  
54  
55  
56  
57  
58  
59  
60

In the present study we decided to combine the ultra-small size of Au NCs (~2 nm) and the multivalency of a mannose ligand in the presence of monocyte-derived DCs. Our aim was to determine the uptake efficiency of this nanosystem and study the mechanism by which Au NCs protected by zwitterionic or a mixture of zwitterionic and carbohydrate (i.e. trivalent mannose) ligands are uptaken (Figure 1). After comprehensively

1  
2  
3 characterising the chemical and optical properties of multivalent mannose-stabilised Au  
4  
5 NCs, cell studies determined a strong increase in DC uptake efficiency due to the  
6  
7 presence of the multivalent mannose ligand. Electron microscopy data indicate that Au  
8  
9 NC uptake in DCs occurs via endocytic pathways with particle accumulation visible in  
10  
11 endosomes and lysosomes. Results from experiments using pharmacological inhibitors of  
12  
13 different cellular pathways confirm the endocytic uptake of Au NCs by multiple pathways  
14  
15 with a strong contribution from clathrin and F-actin dependent mechanisms. The specific  
16  
17 uptake of multivalent mannose stabilised Au NCs by C-lectin receptors was also clearly  
18  
19 demonstrated by a 60% decrease in the presence of mannan, a specific carbohydrate  
20  
21 inhibitor.  
22  
23  
24  
25  
26  
27  
28  
29

## 30 MATERIALS AND METHODS

31  
32  
33  
34 All chemical products were purchased from Sigma Aldrich (Spain). Ultra-pure MilliQ  
35  
36 water was used for all syntheses.  
37  
38  
39

40 **Synthesis of the ligands.** Thioctic-zwitterion (Zw,  $M \sim 412 \text{ g.mol}^{-1}$ ) was synthesized  
41  
42 following the protocol described elsewhere<sup>40, 53</sup>. Synthesis of the dithiol trivalent mannose  
43  
44 linker ( $M \sim 2377 \text{ g.mol}^{-1}$ ) corresponding to 2 monomers, here called TriMan, ( $M \sim 1190$   
45  
46  $\text{g.mol}^{-1}$ ) is reported in the supporting information (refer to Figures S1 and S2 for details of  
47  
48 the synthesis and characterisation by NMR, FTIR and mass spectroscopy).  
49  
50  
51  
52  
53  
54  
55  
56  
57  
58  
59  
60

1  
2  
3 **Synthesis of Au NCs.** Zw ligand-stabilised Au NCs were prepared by adding gold salt  
4 (HAuCl<sub>4</sub>.3H<sub>2</sub>O, 50 mM) to a basic solution (pH 10) containing the ligand in the presence  
5 of NaBH<sub>4</sub> reducing agent (50 mM) and stirred for 15 h. Zwitterion-stabilized Au NCs  
6 (AuZw) were synthesised with a 1:10:2 Au:Zw:NaBH<sub>4</sub> molar ratio. The second type of  
7 NC containing the TriMan co-ligand (AuZwTriMan) was prepared using the same  
8 protocol as used for AuZw plus the dropwise addition of a specific amount of dithio-  
9 TriMan 10 min after the addition of NaBH<sub>4</sub>. The optimum molar ratio for AuZwTriMan  
10 is Au:Zw:NaBH<sub>4</sub>:TriMan= 1:10:2:0.21. Solutions were then dialysed with a 3.5 kDa cut-  
11 off membrane (SnakeSkin, ThermoScientific) for 24 h to remove excess free ligands, then  
12 concentrated to 500 µg gold/mL with Amicon 3 kDa cut-off filters (13,600 rpm; 20 min)  
13 in water and kept refrigerated until use.  
14  
15  
16  
17  
18  
19  
20  
21  
22  
23  
24  
25  
26  
27  
28  
29  
30

31 **NC Characterization.** NMR spectroscopy of AuZw, AuZwTriMan, and of the free  
32 ligands (Zw, TriMan) was performed using a Bruker Ascend™ 400 MHz NMR with  
33 deuterium oxide. Freeze-dried samples were characterized by infrared spectroscopy using  
34 a Jasco FTIR-4100 from 650 cm<sup>-1</sup> to 4000 cm<sup>-1</sup>. PAGE electrophoresis of the NCs:  
35 AuZw, AuZwTriMan on a 15% polyacrylamide gel was carried out using the Bio-Rad  
36 mini-Protean system (Hercules, CA, USA) at 100 V for 120 min. Each well was loaded  
37 with 20 µL of concentrated sample mixed with 10 µL of glycerol. Molecular weight was  
38 determined with a Precision Plus Protein Dual Xtra standard indicator™ (2-250 kDa).  
39 Presence of fragmented gold NCs and TriMan ligand mass were determined by Matrix-  
40 assisted laser desorption/ionization (MALDI) on a 4700 Proteomics Analyzer Mass  
41 Spectrometer (ABSCIEX, Framingham, MA, USA). Samples were prepared with the  
42 matrix  $\alpha$ -Cyano-4-hydroxycinnamic acid (CHCA), 5 mg/mL in 50% acetonitrile, 0.1%  
43  
44  
45  
46  
47  
48  
49  
50  
51  
52  
53  
54  
55  
56  
57  
58  
59  
60



1  
2  
3 trifluoroacetic acid (TFA) with a 1:1 volume ratio. The samples were analysed in  
4 Reflective mode and Linear middle mass positive ion mode: 20 kV source 1 acceleration  
5 voltage. The Grid 1 voltage was set to 92.5% of the source 1 acceleration voltage. Delay  
6 time DE1 was 850 ns, and the low mass gate was enabled with an offset of 0.0. Each data  
7 point was the sum of 20 spectra, acquired with 50 laser shots each. External calibration  
8 was carried out with a set of synthetic peptides (Sequazyme Peptide Mass Standards Kit,  
9 Calibration,Mixture3,ABSCIEX).

10  
11 The metallic and organic composition of samples was determined by thermal and  
12 elemental analysis. Thermal analysis of AuZwTriMan was performed by  
13 Thermogravimetry (TG), and differential scanning calorimetry (DSC) using a METTLER  
14 TOLEDO model TGA/DSC 1 between 30 and 850°C at 10 °C / min with an air flux at 50  
15 mL / min. Elemental analysis was estimated by inductively coupled plasma high  
16 resolution mass spectrometry (ICP-HRMS) on an ELEMENT XS (Thermo Fisher). Gold  
17 and sulphur concentration was determined with Thermo Element software (Thermo  
18 Fisher).

19  
20 Au NC hydrodynamic diameters and zeta potentials in water, PBS buffer and RPMI 1640  
21 + 10% Fetal Calf Serum (FCS) were analysed using a Nano ZS Zetasizer (Malvern).  
22 Absorption spectra over a 190-900 nm range were collected using a Cary 100 Bio UV-  
23 visible spectrophotometer (Varian). Steady-state fluorescence measurements were  
24 obtained with diluted samples on a Perkin Elmer LS45 Fluorescence Spectrometer.  
25 Fluorescence lifetime measurements were carried out on an Edinburgh Instruments  
26 FLS920 fluorometer equipped with an EPL-375 Edinburgh Instrument laser. Spectra were  
27  
28  
29  
30  
31  
32  
33  
34  
35  
36  
37  
38  
39  
40  
41  
42  
43  
44  
45  
46  
47  
48  
49  
50  
51  
52  
53  
54  
55  
56  
57  
58  
59  
60

1  
2  
3 registered with excitation at 374.65 nm and emission detected at 680 nm (slits= 8 nm).  
4  
5  
6  
7  
8

9  
10 **Generation of Monocyte-Derived DCs.** Fresh peripheral blood mononuclear cells,  
11 obtained from 40 mL of blood per individual, were used for monocyte purification by  
12 means of anti-CD14 microbeads following the manufacturer's protocol (Miltenyi Biotec,  
13 Germany). The CD14<sup>-</sup> cell fraction was placed in 10% dimethyl sulfoxide and frozen for  
14 a later lymphocyte proliferation test. To generate DCs, monocytes (CD14<sup>+</sup> cells) were  
15 incubated in complete medium (CM) containing Roswell Park Memorial Institute 1640  
16 medium (Life Technologies, USA) supplemented with 10% Fetal Calf Serum (FCS; Life  
17 Technologies, USA), streptomycin (100  $\mu\text{g}\cdot\text{mL}^{-1}$ ), gentamicin (1.25  $\text{U}\cdot\text{mL}^{-1}$ ) as well as  
18 recombinant human rhGM-CSF (200  $\text{ng}\cdot\text{mL}^{-1}$ ) and rhIL-4 (100  $\text{ng}\cdot\text{mL}^{-1}$ ) (both from R&D  
19 Systems Inc., USA) for 5 days at 37°C and 5% CO<sub>2</sub>. The resulting DCs were then  
20 recovered and used in the experiments.  
21  
22  
23  
24  
25  
26  
27  
28  
29  
30  
31  
32  
33  
34  
35  
36

37 **Gold concentration in DCs.** Quantification of Au NCs in DCs was estimated by  
38 inductively coupled plasma high resolution mass spectrometry (ICP-HRMS) on an  
39 ELEMENT XS (Thermo Fisher) after digesting cells (average of 70,000 cells per sample)  
40 with strong acid. Gold concentration in  $\mu\text{g}/\text{L}$  was determined with Thermo Element  
41 software (Thermo Fisher).  
42  
43  
44  
45  
46  
47  
48  
49  
50  
51  
52

53 **Flow cytometry-based detection of Au NC-containing DCs.** DCs were incubated at  
54  $1\times 10^5$  cells/well in 96-well plates (Nunc, Roskilde, Denmark) with Au NCs at 1, 5, 10 and  
55  
56  
57  
58  
59  
60

1  
2  
3 25  $\mu\text{g.mL}^{-1}$  concentrations in CM for 3 h and 48 h at 37 °C. Cells were then analyzed  
4  
5 using a FACSCanto II flow cytometer (BD Biosciences, USA) selecting a detection  
6  
7 window between 720 and 860 nm, and the data processed using FLOWJO software (Tree  
8  
9 Star, Inc, USA).  
10  
11

12  
13  
14 **Cell Toxicity Analyses.** The cytotoxic effects of Au NCs on DCs were determined by  
15  
16 flow cytometry. Typically,  $1 \times 10^5$  of DCs were incubated with NCs at 1, 5, 10 and 25  
17  
18  $\mu\text{g.mL}^{-1}$  in CM for 48 h at 37 °C and 5% CO<sub>2</sub>. After incubation, cells were stained with  
19  
20 Live/Dead NearIR (Life Technologies-Invitrogen, USA) for 15–20 min. Cells were then  
21  
22 assessed by flow cytometry (FACSCanto II flow cytometer, BD Biosciences, USA) using  
23  
24 a laser excitation wavelength of 633 nm to measure the distribution of fluorescence  
25  
26 emissions. Data were analysed using FLOWJO software (Tree Star, Inc, USA). The  
27  
28 cytotoxicity of NCs on DCs are expressed as a percentage of live cells in experimental  
29  
30 samples versus untreated cells.  
31  
32  
33  
34  
35  
36

37  
38 **Ethical Statement.** This study was approved by the institutional review board “Comisión  
39  
40 de Ética y de Investigación del Hospital Regional Universitario de Málaga”, and the  
41  
42 experiments carried out in accordance with the Declaration of Helsinki. Oral and written  
43  
44 informed consents for all the procedures were obtained from the subjects included in the  
45  
46 study.  
47  
48

49  
50 **Confocal Laser Microscopy (CLSM).** Following incubation with Au NCs, DCs were  
51  
52 fixed in PBS containing 4% paraformaldehyde for 1 hour, washed three times with PBS  
53  
54 and stored protected from light at 4 °C until analysis. Sub-membrane actin and Nuclei  
55  
56 (DNA) were labelled by ~20 minute incubations with 10  $\mu\text{M}$  Atto488-conjugated  
57  
58  
59  
60

1  
2  
3 Phalloidin (Sigma) and 1  $\mu\text{g/ml}$  Hoechst 33258 (Sigma), respectively. Once prepared,  
4  
5 DCs were either mounted on glass slides in Fluoroshield mounting medium (Sigma) or  
6  
7 transferred to optical bottom 96 well plates (Nunc) in PBS for observation by CLSM. For  
8  
9 the lysosome staining, after fixation, cells were permeabilised with saponin (0.1% in PBS  
10  
11 with 2% Bovine Serum Albumin V fraction (Sigma) followed by an overnight incubation  
12  
13 at 4°C with the primary rabbit LAMP-1 (Santa Cruz Biotechnology) antibody using a  
14  
15 1:25 dilution followed by a 1 h incubation at room temperature with a secondary anti-  
16  
17 rabbit Cy2-conjugated antibody (Jackson Laboratories). Cells were washed three times  
18  
19 after each antibody incubation and finally mounted on glass slides. Samples were  
20  
21 analysed using a Leica DM6000 inverted microscope connected to a Leica SP5 laser  
22  
23 scanning confocal system. For the calculation of Au NC fluorescence intensities, single  
24  
25 optical sections were captured from unstained DCs using excitation at 488 nm and  
26  
27 detection of Au NC fluorescence emissions between 580-700 nm, with an independent  
28  
29 brightfield channel (transmitted light) to allow cell detection. For DCs stained with  
30  
31 phalloidin, ATTO488 and Au NC fluorescence were detected simultaneously using 488  
32  
33 nm excitation with a  $\sim$ 495-520 nm detection window for ATTO488 and  $\sim$ 600-700 nm for  
34  
35 Au NCs (red shifted to avoid cross-talk from ATTO488). Hoechst 33258 was measured  
36  
37 using 405 nm excitation with a 415-470 nm detection window (measured sequentially to  
38  
39 avoid crosstalk in other channels).  
40  
41  
42  
43  
44  
45  
46  
47  
48  
49

50 **Transmission Electron Microscopy (TEM).** Au NC images were obtained on a FEI  
51  
52 Tecnai G2 Twin TEM at 200 kV. TEM samples were prepared by placing a drop of Au  
53  
54 NC solution onto a copper grid covered with holey carbon films. Briefly, cells were fixed  
55  
56 in a mixture of 2% paraformaldehyde-2.5% glutaraldehyde-0.2 M sucrose in PB at 4°C,  
57  
58  
59  
60

1  
2  
3 overnight. After centrifugation, cell pellets were embedded in 10% gelatin, which was  
4  
5 solidified at 4°C and cut into small blocks. After washing with PB, blocks were post-fixed  
6  
7 in 1% buffered osmium tetroxide for 1 h at room temperature, rinsed in distilled water  
8  
9 and dehydrated in an ethanol series, followed by embedding in low viscosity Spurr's resin  
10  
11 (Electron Microscopy Sciences). Ultrathin sections (70 nm) were obtained with a Leica  
12  
13 EM UC-7 ultramicrotome at room temperature. Electron micrographs were obtained in a  
14  
15 Tecnai G2 20 Twin (FEI) at 100 kV, with a 4 megapixels Veleta wide-angle camera  
16  
17 (Olympus) for general imaging, and a 16 megapixel Eagle on-axis camera (FEI) for high  
18  
19 resolution images, using TIA software (FEI).  
20  
21  
22  
23  
24  
25

26 **Cell experiment with pharmacological inhibitors.** To study the mechanism involved in  
27  
28 Au NC uptake, we selected the following inhibitors and experimentally-determined their  
29  
30 optimal concentrations: 5  $\mu\text{g.mL}^{-1}$  (10  $\mu\text{M}$ ) cytochalasin D (CytD), 10  $\mu\text{g.mL}^{-1}$  (25  $\mu\text{M}$ )  
31  
32 5-(N-ethyl-N-isopropyl)hydrochloride (EIPA), 10  $\mu\text{g.mL}^{-1}$  (33  $\mu\text{M}$ ) nocodazole, 10  
33  
34  $\mu\text{g.mL}^{-1}$  (28.1  $\mu\text{M}$ ) chlorpromazine hydrochloride, 10  $\mu\text{g.mL}^{-1}$  (40 $\mu\text{M}$ ) dynasore, 100  
35  
36  $\mu\text{g.mL}^{-1}$  mannan.  $6 \times 10^5$  DCs/well were first pre-treated with the different inhibitors for  
37  
38 30 min and then incubated with Au NCs at 10 and 25  $\mu\text{g/mL}$  concentrations for 8 h in CM  
39  
40 at 37 °C. Cells were analysed by flow cytometry and confocal microscopy using the same  
41  
42 settings as described for the concentration experiment. Toxicity tests in the presence of  
43  
44 the inhibitors were performed with the Live/Dead NearIR stain. Data were obtained from  
45  
46 two independent sets of experiments each using cells from three different patients.  
47  
48  
49  
50  
51  
52  
53  
54

## 55 **RESULTS & DISCUSSION**

56  
57  
58  
59  
60

**Au NC characterisation.** The NCs AuZw and AuZwTriMan were prepared according to the crystal growth/reduction method using zwitterionic thiol (Zw) and trivalent mannose derivative (TriMan) molecules as protecting agents (Figure 1).

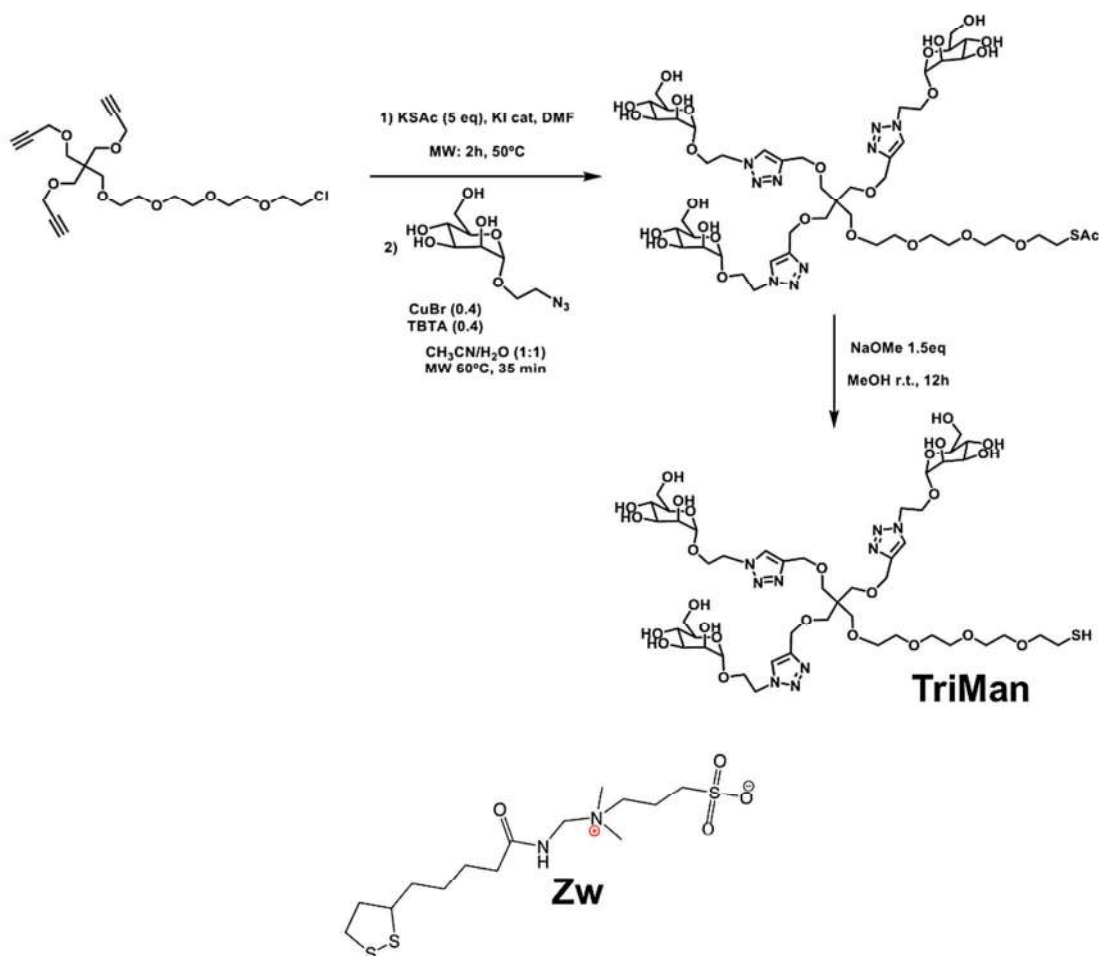


Figure 1. Synthetic steps for the preparation of the trivalent mannose compound (TriMan) and the chemical formula of the thioctic zwitterion compound (Zw).

Both TriMan and Zw can interact with gold species via their mono or bidentate thiol groups, respectively. Due to the high molar Au:Ligand ratio used during synthesis,

1  
2  
3 dialysis was performed to remove remaining free ligand and prevent self-aggregation of  
4 the thiolated ligands. Spectroscopic analyses of AuZwTriMan by NMR and FTIR  
5 (Figures S3, S4) confirmed the presence of the zwitterionic and carbohydrate molecules.  
6  
7  
8  
9  
10 Mass spectrometry (MALDI-Tof) experiments were performed on AuZw and  
11 AuZwTriMan samples using reflective and linear positive modes to obtain information on  
12 the carbohydrate ligand and the Au NCs, respectively. Our measurements in reflective  
13 mode detected the monomer signal for the trivalent mannose ligand at  $m/z = 1190.35$  with  
14 a small amount of the initial dithiol mannose compound ligand at  $m/z = 2377.66$ ,  
15 indicating the reduction of the dimers during synthesis (Figure S5). The measurements  
16 carried out in linear mode confirmed the presence of multiple peaks corresponding to  
17 fragmented AuZw and AuZwTriMan NCs in the same mass range, with a maximum mass  
18 of  $m/z \sim 7000$  (Figure S6). This may indicate a similar size or structure for both NCs,  
19 where the low amount of carbohydrate added for the synthesis of AuZwTriMan does not  
20 seem to significantly influence NC growth. However, we observed a shift of the broad  
21 band centered from  $\sim 14$  kDa for AuZw to  $\sim 17$  kDa for AuZwTriMan. This band most  
22 likely corresponds to ligand stabilized-Au NCs with the higher molecular weight of  
23 TriMan versus Zw explaining the size difference. PAGE electrophoresis revealed that  
24 both fluorescent NCs migrate at  $\sim 10$  kDa but with a slightly higher size distribution for  
25 AuZwTriMan (Figure S7). This observation seems to be in agreement with the mass  
26 spectrometry measurements. It should be noted that species  $> 10$  kDa were not visible by  
27 UV illumination, suggesting that these larger particles emit little or no fluorescence.  
28  
29  
30  
31  
32  
33  
34  
35  
36  
37  
38  
39  
40  
41  
42  
43  
44  
45  
46  
47  
48  
49  
50  
51  
52  
53  
54  
55  
56  
57  
58  
59  
60  
Chemical analyses of AuZwTriMan and AuZw by thermogravimetry and elemental  
analysis are shown in Table 1.

	Wt.% organic moiety*	Wt. % of Man**	Au:S***	Molecular weight****
<i>AuZw</i>	80±3	0	1:8.9	~14kDa
<i>AuZwTriMan</i>	83±3	8±2	1:12.5	~17kDa

\*: determined by thermogravimetry; \*\*: determined by anthrone test; \*\*\*: measurements performed by ICP; \*\*\*\*: Value estimated for the fluorescent Au NCs by MALDI/Tof analyses.

Table 1. Chemical characterisation of the AuZwTriMan and AuZw NCs.

Our results show the high organic moiety of the sample AuZwTriMan (> 80wt.%) and an Au:S molar ratio of 1:12.5, which is significantly higher than the 1:1 ratio suggested by the formation of organic multilayers stabilized by covalent (disulfide) and electrostatic interactions on the metal surface similar to previously reported supramolecular assemblies<sup>36</sup>. To quantify the amount of TriMan carbohydrate in AuZwTriMan NCs, we used the colourimetric anthrone test (Figure S8), which determined that trivalent mannose accounts for approximately 8% of total organic weight. Transmission electronic microscopy (TEM) images of AuZwTriMan and AuZw (Figure S9) showed only particles with diameters < 3 nm. Dynamic light scattering (DLS) confirmed the small size of AuZw ( $\text{\O} = 1.3 \pm 0.5$  nm) and AuZwTriMan ( $\text{\O} = 2.7 \pm 0.5$  nm) in water (Figure 2a). Zeta potential for AuZw and AuZwTriMan were similar in water and in PBS buffer (10 mM; pH 7.4) with values around -20 mV. The negative charge of the Au NCs could be attributed to the presence of sulphur trioxide from Zw and hydroxyl groups from TriMan.



1  
2  
3 Lowering the pH to 4, resulted in neutral AuZwTriMan species and even slightly  
4 positively charged ones in the case of AuZw, but this did not generate detectable  
5 precipitation from either NC over a period of 6 months (data not shown). This suggests  
6 that both NCs possess strong colloidal stability.  
7  
8  
9  
10  
11

12  
13  
14 The optical features of AuZwTriMan sol are similar to AuZw (Figures 2b) with a broad  
15 fluorescence emission in the red-NIR region ( $\lambda_{em.} = 680$  nm) and the presence of multiple  
16 excitation bands (370, 400, 450, 490, and 515 nm) associated with intra and inter energy  
17 electronic transitions. Such broad emissions are quite common for Au NCs and are related  
18 to the presence of multiple atomic species. We found that high TriMan concentrations  
19 resulted in decreased fluorescence intensities (Figure S10). Therefore, we determined an  
20 optimal Au:Zw:NaBH<sub>4</sub>:TriMan ratio of 1:10:2:0.21, which resulted in a relatively high  
21 level of fluorescence with an intensity loss less than 20% with respect to AuZw and  
22 colloidal stability in vitro. The effect of high TriMan concentrations could be attributed to  
23 strong interactions between Au<sup>III</sup> and TriMan OH groups and TriMan's large size relative  
24 to Zw causing steric hindrance that prevents the growth of fluorescent Au NCs. The  
25 relative amounts of two different ligands have recently been shown to influence the size  
26 and shell structure of Ag-doped-Au NCs, dramatically affecting their optical properties<sup>54</sup>.  
27  
28 The red-shift of AuZwTriMan fluorescence could be attributed either to an altered  
29 average core size, according to the jellium model<sup>32</sup>, or to changes to the metal surface  
30 following addition of the carbohydrate ligand. Indeed, with respect to the latter  
31 possibility, several studies have shown that ligand nature can affect red-NIR region  
32 photoluminescence<sup>38, 55</sup>. The excitation peaks for the two Au NCs are similarly located to  
33 those reported for other Au NCs stabilised by thiol linkers regardless of the terminal  
34  
35  
36  
37  
38  
39  
40  
41  
42  
43  
44  
45  
46  
47  
48  
49  
50  
51  
52  
53  
54  
55  
56  
57  
58  
59  
60

groups used<sup>55</sup>. The absorbance spectra of AuZwTriMan and AuZw sols show strong UV absorption with the presence of broad and weak bands between 400 and 500 nm (Figure 2c). Fluorescence lifetime measurements of AuZwTriMan in water show a biexponential behaviour of  $\tau_1 = 300$  ns (15%) and  $\tau_2 = 1.5$   $\mu$ s (85%) with a microsecond range lifetime characteristic of the metal-ligand electronic transition (Figure 2d)<sup>44, 56</sup>. The short nanosecond range lifetime is usually associated with singlet excited states originating from metal-metal interactions. On the other hand, the long microsecond range lifetime component is typical of triplet excited states<sup>43, 57</sup>. This extended high energy state is of interest for analytical applications due to its high sensitivity to the local environment. The most important optical features of AuZw and AuZwTriMan are summarised in Table 2.

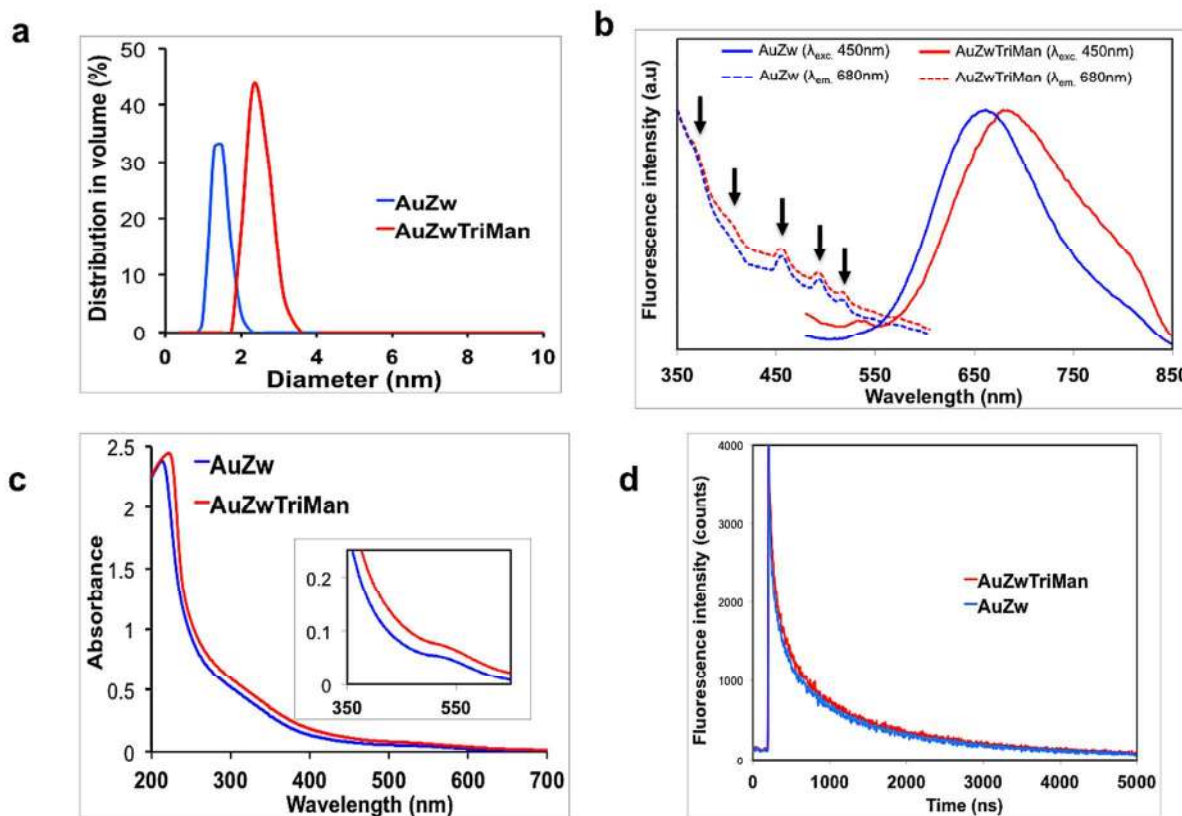


Figure 2. (a) Size measurements of AuZw and AuZwTriMan in water by dynamic light scattering (DLS). (b) Excitation (dashed line;  $\lambda_{em.} = 680$  nm) and emission (solid line;  $\lambda_{exc.} = 450$  nm) spectra of AuZwTriMan and AuZw dispersed in water. Both Au NCs emitted in

the red-NIR window with the typical multiple excitation peaks (370, 405, 470, 495 nm: arrows) of Au NCs. (c) The absorbance profiles of diluted AuZw and AuZwTriMan solutions exhibited strong absorbance in the UV region and a shoulder between 400 and 500 nm (inset). (d) Fluorescence lifetime decay of AuZwTriMan and AuZw sols.  $\lambda_{exc./\lambda_{em.}} = 374.8$  nm/680 nm.

	$\lambda_{em.}^*$	Relative fluorescence intensity**		Lifetime		$\phi^{***}$
		Water	PBS (10mM, pH 7.2)	Water	PBS (10mM, pH 7.2)	
<i>AuZw</i>	665nm	1	0.97	$\tau_1=1.53\mu\text{s}$ (85%); $\tau_2=312\text{ns}$ (15%)	$\tau_1=1.93\mu\text{s}$ (73%); $\tau_2=529\text{ns}$ (27%)	11.3
<i>AuZwTriMan</i>	680nm	0.89	0.79	$\tau_1=1.50\mu\text{s}$ (85%); $\tau_2=300\text{ns}$ (15%)	$\tau_1=1.90\mu\text{s}$ (69%); $\tau_2=541\text{ns}$ (27%)	8.7

\* $\lambda_{exc.}=450\text{nm}$ ; \*\*: normalised to AuZw fluorescence intensity. Both NCs have an absorbance of 0.1 at  $\lambda_{exc.}=450\text{nm}$ ; \*\*\* determined by comparison with Fluorescein ( $\phi=0.79$  in 0.1M NaOH).

Table 2. Optical properties of the AuZwTriMan and AuZw NCs.

In order to verify the activity of the trivalent mannose present on the surface of the AuZwTriMan metal core, a simple test was performed by adding the lectin concanavalin A (ConA,  $5 \text{ mg}\cdot\text{mL}^{-1}$ ) to diluted sols of AuZw and AuZwTriMan in PBS buffer (10 mM; pH 7.4) in the presence of calcium and magnesium ions ( $(\text{Ca}^{2+}) = (\text{Mn}^{2+}) = 0.1 \text{ mM}$ ). Only AuZwTriMan became more turbid in the presence of ConA, indicating aggregate formation (data not shown). AuZw fluorescence decreased evenly upon adding ConA (Figure 3a). In contrast, the addition of ConA increased AuZwTriMan fluorescence at  $\lambda = 685\text{nm}$ , accompanied by a small red shift (Figure 3b). Aggregation-induced increases in fluorescence intensity at shorter wavelengths have recently been reported<sup>45</sup>. The phenomenon of aggregation induced emission (AIE) is well documented for organic luminophores<sup>58</sup> but has only recently been reported for metal (Au, Cu) nanoclusters<sup>45, 59</sup>.

1  
2  
3 For instance, in an elegant study from the Xie laboratory it was shown that Au NC  
4 aggregation induced by the presence of ethanol or by electrostatic interactions in the  
5 presence of cadmium cations led to a drastic fluorescent enhancement<sup>45</sup>. It was proposed  
6 that the strong fluorescence of the dense aggregates was generated by both inter/intra  
7 complex aurophilic interactions and by the reduced intramolecular motion of the  
8 complex. In our case, the AIE of AuZwTriMan emissions are likely to be the result of  
9 electrostatic interactions between the lectin and the carbohydrate ligand as the NC core is  
10 strongly protected by a saturation of mono and bidentate thiol ligands.  
11  
12  
13  
14  
15  
16  
17  
18  
19  
20  
21  
22  
23

24 We expected that the long fluorescence lifetime of Au NCs would be sensitive to their  
25 aggregation state. Indeed, their fluorescence lifetime was longer in PBS buffer than in  
26 deionized water (Table 2) probably due to Au NC crosslinking induced by the presence of  
27 salts. Moreover, we found that the microsecond range ( $\tau_2$ ) fluorescence lifetime of  
28 AuZwTriMan was strongly influenced by the presence of ConA, dropping from 1.91  $\mu$ s to  
29 1.51  $\mu$ s, while no change was observed for AuZw (Figure 3c). This decrease could be  
30 attributed to the combined contribution of NC local polarity changes and enhanced  
31 network rigidity induced by the formation of dense aggregates. The NC crosslinking  
32 hypothesis is consistent with the altered excitation spectrum profile of AuZwTriMan in  
33 the presence of ConA (Figure 3d). In fact, the AuZwTriMan  $\lambda = 450$  nm excitation peak  
34 increased significantly relative the AuZw equivalent, as well as the appearance of two  
35 new peaks at longer wavelength ( $\lambda = 545$  nm;  $\lambda = 575$  nm). The 450 nm band has been  
36 mainly associated with different gold magic cluster to electronic interband transitions  
37 ( $sp \leftarrow d$ ) that are strongly involved in ligand-to-metal charge transfers (LMCTs) or ligand  
38 to metal-metal charge transfers (LMMCTs)<sup>55</sup>. Therefore, the aggregation triggered by  
39  
40  
41  
42  
43  
44  
45  
46  
47  
48  
49  
50  
51  
52  
53  
54  
55  
56  
57  
58  
59  
60

1  
2  
3  
4  
5  
6  
7  
8  
9  
10  
11  
12  
13  
14  
15  
16  
17  
18  
19  
20  
21  
22  
23  
24  
25  
26  
27  
28  
29  
30  
31  
32  
33  
34  
35  
36  
37  
38  
39  
40  
41  
42  
43  
44  
45  
46  
47  
48  
49  
50  
51  
52  
53  
54  
55  
56  
57  
58  
59  
60

ConA could be responsible for a rearrangement of the polymeric monolayer that protects the NC gold core. However, the complexity of the photoluminescence mechanisms occurring in this system via multiple intra and inter electronic transitions will require further investigation, especially by looking at the properties of monodisperse single metal NCs. In summary, the enhanced fluorescence emissions and decreased fluorescence lifetime of AuZwTriMan are consistent with its aggregation in the presence of ConA, confirming specific binding between lectin and the carbohydrate ligand.

The colloidal stability of AuZwTriMan and AuZw dispersed in CM (RPMI1640 + 10% FCS) was determined by DLS over 48 h. Particles rapidly increased to  $\approx 10$  nm, probably due to protein corona formation, but did not show any significant aggregation (Figure S11). The presence of protein in the CM influenced Au NC surface charge with their zeta potential shifting from -20 mV to -10 mV. Fluorescence measurements carried out in CM confirmed the relatively high optical stability of both NCs (Figure S12) over 48 h.

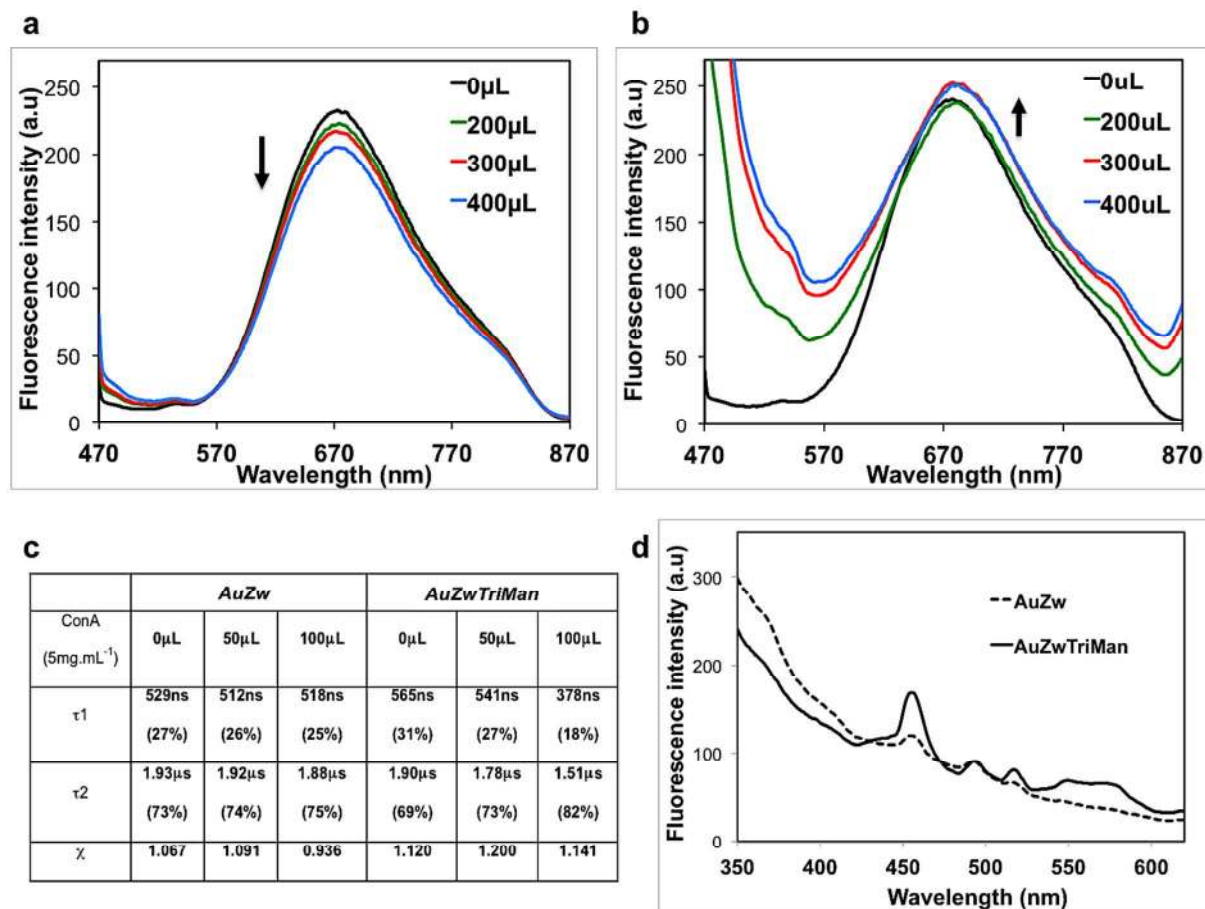


Figure 3. Fluorescence emission of AuZw (a) and AuZwTriMan (b) dispersed in PBS buffer (10 mM; pH 7.4) with ( $\text{Ca}^{2+} = \text{Mn}^{2+} = 0.1 \text{ mM}$ ) after the addition of ConA (5 mg.mL<sup>-1</sup>).  $\lambda_{\text{exc.}} = 450\text{nm}$ . (c) Fluorescence lifetime data of AuZw and AuZwTriMan in the presence of ConA (5 mg. mL<sup>-1</sup>) under the same conditions as previously described.  $\lambda_{\text{exc.}} = 374.65\text{nm}$ ;  $\lambda_{\text{em.}} = 680 \text{ nm}$ . (d) Excitation spectra of AuZw (dashed line) and AuZwTriMan (solid line) after the addition of ConA (5 mg.mL<sup>-1</sup>).  $\lambda_{\text{em.}} = 680\text{nm}$ .

**Au NC cellular accumulation.** In order to determine the influence of the trivalent mannose linker on Au NC-DC interactions, different concentrations of AuZwTriMan and AuZw from 1  $\mu\text{g.mL}^{-1}$  to 25  $\mu\text{g.mL}^{-1}$  were incubated with DCs for 3 h or 48 h and studied by several techniques. Au NCs could be quantified and localised by flow cytometry and Confocal Laser Scanning Microscopy (CLSM) even at low concentrations thanks to their fluorescence emission in the NIR region and high Stokes-shift<sup>41, 44</sup>. Flow cytometry

1  
2  
3 measurements shown in Figure 4a indicate that AuZwTriMan and AuZw were uptaken by  
4 DCs in a dose dependent manner after 48 h. However, the uptake of AuZwTriMan NCs  
5 was 62% (1.62 fold) stronger than for AuZw at 1  $\mu\text{g.mL}^{-1}$  gold concentration and by  
6 256% (3.56 fold) at 25  $\mu\text{g.mL}^{-1}$ . These results strongly suggest that the presence of  
7 TriMan promotes NC enhanced uptake in DCs. However, as fluorescence might be  
8 affected by the local cellular environment (pH, particle aggregation etc.), we also  
9 measured the gold concentration in DCs following incubation with AuZw and  
10 AuZwTriMan by Inductively Coupled Plasma (ICP) analysis. This analysis confirmed a  
11 higher gold concentration (> 75%) in cells incubated with the glyco-Au NC (Figure S13).  
12 These results clearly demonstrate a strong enhancement of dendritic cell NC uptake by  
13 the presence of the trivalent mannose ligand. Additional experiments found that DC  
14 uptake of both AuZwTriMan and AuZw Au NCs continues to increase after 3 h, with  
15 higher levels of fluorescence detected after 48 h under most conditions (Figure S14).  
16 Interestingly, in the case of AuZwTriMan, more than 50% of cells exhibited detectable  
17 fluorescence after 3h (versus only 12% for AuZw) even at the lower Au NC  
18 concentration. The CLSM images, shown in Figure 4b, indicate that NCs were distributed  
19 homogeneously in the cells and confirm the flow cytometry data with a higher uptake of  
20 AuZwTriMan than AuZw in DCs at 5 and 10  $\mu\text{g.mL}^{-1}$  concentrations after 48 h.  
21  
22  
23  
24  
25  
26  
27  
28  
29  
30  
31  
32  
33  
34  
35  
36  
37  
38  
39  
40  
41  
42  
43  
44  
45  
46  
47  
48  
49  
50  
51  
52  
53  
54  
55  
56  
57  
58  
59  
60

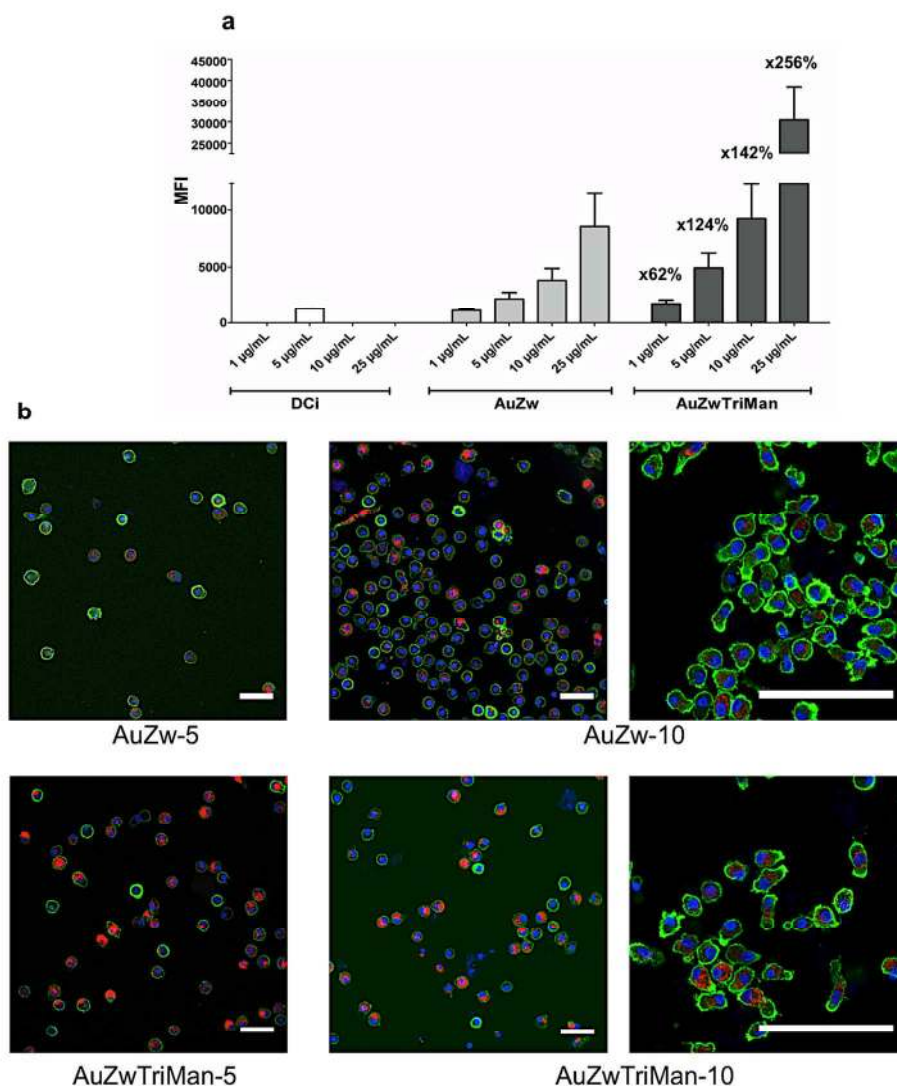


Figure 4. (a) Flow cytometry measurements of DCs incubated with AuZw and AuZwTriMan at different concentrations (1, 5, 10, and 25  $\mu\text{g}\cdot\text{mL}^{-1}$  in CM) for 48 h. MFI: mean fluorescence intensity. Results showed the strong enhancement of particle uptake for Au NCs containing the mannose ligand. (b) CLSM images of DCs incubated with AuZw and AuZwTriMan at 5 and 10  $\mu\text{g}\cdot\text{mL}^{-1}$  in CM for 48 h. Bars: 100  $\mu\text{m}$ . Data are consistent with the flow cytometry analysis showing a higher fluorescence signal (red) from AuZwTriMan than for AuZw inside the cells at the same concentration. Sub-membrane actin was stained post-fixation with ATTO488-phalloidin (green) and nuclei with Hoechst (blue).



1  
2  
3 The intracellular distribution of red-NIR emitting Au NCs in DCs as determined by  
4 CLSM (Figure S15) appeared similarly independent of the nature of the ligand, with both  
5 particles showing intracellular accumulation in the cytoplasm and strong perinuclear  
6 accumulation as previously reported by our lab<sup>52</sup>. Because both NCs contain a high  
7 content of zwitterionic ligand on their surface, the interaction between the particles and  
8 DCs will involve mainly electrostatic interactions<sup>53</sup>. TEM micrographs of DCs incubated  
9 with AuZwTriMan (25  $\mu\text{g}\cdot\text{mL}^{-1}$  for 48 h) show an accumulation of Au NCs (dark dots  
10 about  $\approx 2$  nm in size) in different organelles (Figure 5 a, b, c; S16). Based on comparisons  
11 with previous particle localisation studies in DCs<sup>60-61</sup> we identified AuZwTriMan NCs in  
12 early endosomes (a), late endosomes (a, e) and lysosomes (d, e) close to the Golgi  
13 apparatus (e), which is consistent with their uptake via endocytic pathways. Experiments  
14 with the lysosome marker LAMP-1 indicate that a relatively low proportion of Au NCs  
15 colocalise with lysosomes (Figure 5f). However, it is important to point out that only  
16 fluorescence from relatively large NC aggregates is likely to be detectable by confocal  
17 microscopy.

18  
19  
20  
21  
22  
23  
24  
25  
26  
27  
28  
29  
30  
31  
32  
33  
34  
35  
36  
37  
38  
39  
40  
41 **Cell toxicity.** Next we incubated AuZw and AuZwTriMan with DCs at different  
42 concentrations (1  $\mu\text{g}\cdot\text{mL}^{-1}$ - 25  $\mu\text{g}\cdot\text{mL}^{-1}$ ) and different incubation times (3 h and 48 h).  
43 Cytometry-based live/dead cell viability assays did not detect any significant toxicity  
44 above the threshold by flow cytometry measurement in any of the tested conditions (data  
45 not shown). This is consistent with absence of Au NC cytotoxicity described in previous  
46 studies using several in vitro and in vivo models<sup>49-50</sup>.

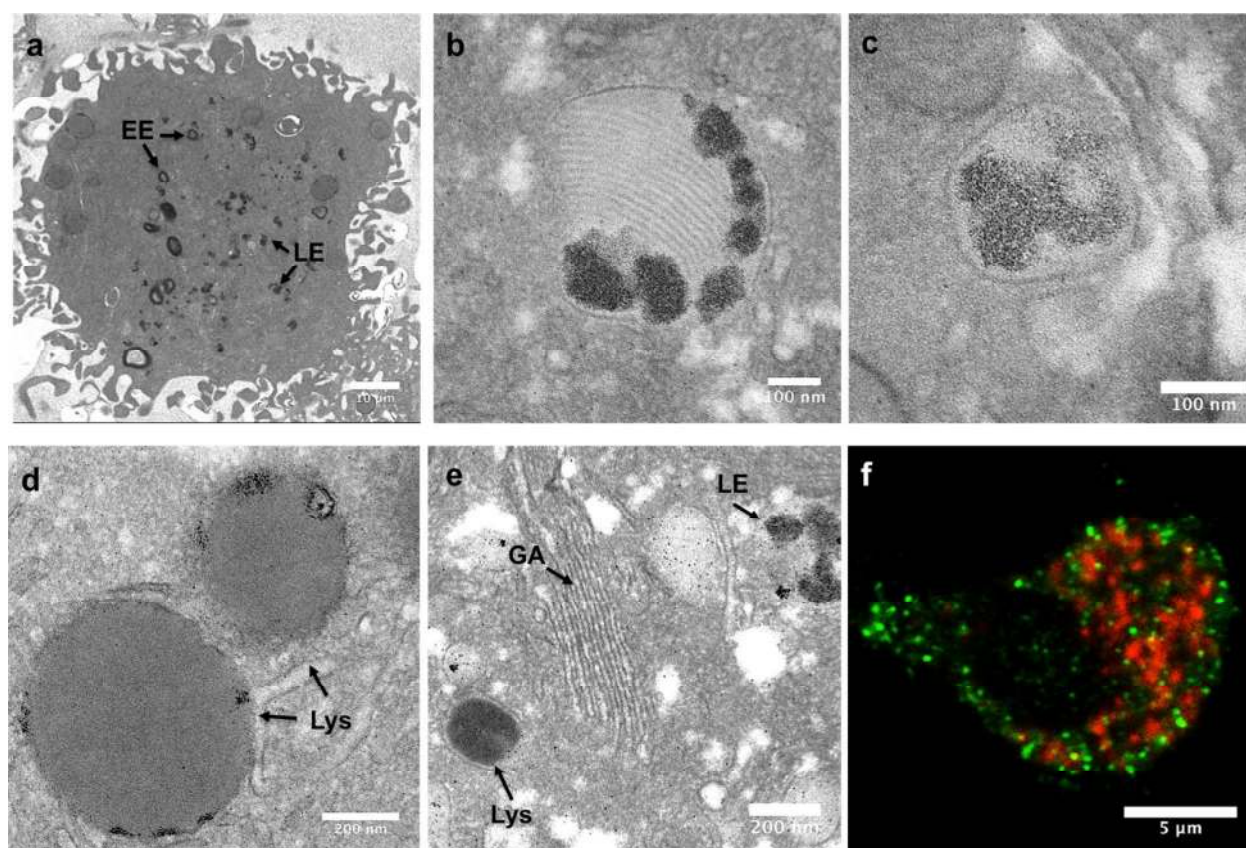
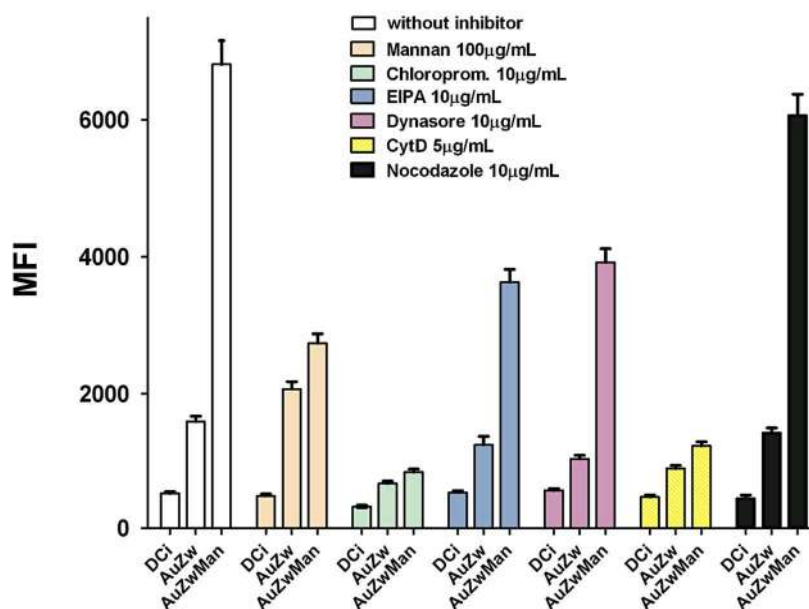


Figure 5. Electron microscopy images of DCs incubated with AuZwTriMan ( $25 \mu\text{g}\cdot\text{mL}^{-1}$  in CM for 48 h) showing the presence of Au NCs (dark dots) in several types of multilaminar and amorphous organelles (a, b, c) from early endosomes (EE) (a) and late endosomes (LE) (a, e) to lysosomes (Lys) (d, e) close to the Golgi apparatus (GA) (e). CLSM image of DCs incubated with AuZwTriMan (red), (f) stained with anti-LAMP-1 (lysosome marker, green) indicating that few LAMP1-positive lysosomes contain detectable levels of AuZwTriMan.

**Au NC uptake mechanisms.** Endocytosis refers to a conserved process whereby macromolecules or solutes are taken up by cells via the invagination of plasma membrane to form vesicles<sup>62</sup>. NPs with size  $< 200$  nm are usually uptaken via endocytic pathways that can be divided into different classes: clathrin-dependent, caveolae, macropinocytosis, and clathrin- and caveolae-independent endocytosis<sup>63</sup>. After endocytosis, NPs tend to be

1  
2  
3 contained within different types of intracellular vesicles, some of which can subsequently  
4 fuse with lysosomes where they accumulate until they are eventually degraded<sup>63</sup>. It has  
5 been established that cellular NP uptake mechanisms are dependent on the physico-  
6 chemical parameters (size, shape, charge, hydrophobicity) of NPs, and on the cell type  
7 studied. To gain more insight into the mechanisms involved in DC uptake of Au NCs  
8 stabilised by the Zw and TriMan ligands, we selected a series of different inhibitors that  
9 differentially affect the endocytic pathways mentioned above. To optimise inhibitor  
10 concentration we first tested different levels of each inhibitor with DCs, with and without  
11 Au NPs, and selected the highest concentration that did not induce detectable cytotoxicity  
12 (Figure S17; data not shown). CLSM was also used to ensure an intact cell cytoskeleton  
13 (except for actin and tubulin depolymerisation using CytD and nocodazole, respectively)  
14 at different concentrations (Figure S18; data not shown). We selected an 8 h Au NC  
15 incubation time as a compromise between a short incubation time to avoid multiple  
16 uptake mechanisms and having enough fluorescent signal for cell analysis.



1  
2  
3  
4  
5 Figure 6. Endocytic pathway inhibitor experiments. DCs were pre-treated with the  
6 inhibitors for 30 min and then incubated for 8h with either AuZw or AuZwTriMan (25  
7  $\mu\text{g.mL}^{-1}$  in CM). Fluorescence was measured by flow cytometry and expressed as mean  
8 fluorescence intensity (MFI).  
9

10  
11  
12  
13  
14  
15  
16 The inhibitor experiments showed consistent results using 10 and 25  $\mu\text{g.mL}^{-1}$  of Au NCs  
17 indicating no saturation of cell uptake in this particle concentration range (Figure S19).  
18  
19 Mannan is a compound commonly chosen as an inhibitor to confirm specific cell uptake  
20 by C-lectin receptors such as MR and DC-SIGN. Flow cytometry measurements showed  
21 a 60% reduction in Au NC uptake for AuZwTriMan (Figure 6), while mannan had no  
22 effect on AuZw uptake. These data clearly demonstrate the highly specific uptake of  
23 AuZwTriMan by C-lectin receptors. This is consistent with the well-known interaction  
24 between mannose molecules and the different types of C-lectin receptor (MR, DC SIGN)  
25 present on the DC surface<sup>61</sup>. The remarkable C-lectin dependent uptake of AuZwTriMan  
26 by DCs might also be attributed to the strong affinity of DC lectin receptors for the  
27 multivalent TriMan ligand.  
28  
29  
30  
31  
32  
33  
34  
35  
36  
37  
38  
39  
40  
41  
42  
43  
44  
45

46 A second inhibitor, chlorpromazine hydrochloride was used to determine if Au NCs are  
47 processed by clathrin-mediated endocytosis (CME). Chlorpromazine is a cationic  
48 amphiphilic class drug and an inhibitor of the clathrin-coated pit pathway.  
49 Chlorpromazine is known to cause a loss of coated pits and associated receptors from the  
50 cell surface, and result in the accumulation of clathrin and AP-2 in endosomal  
51  
52  
53  
54  
55  
56  
57  
58  
59  
60

1  
2  
3 compartments<sup>64</sup>. Results showed 88% and 57% decreases for AuZwTriMan and AuZw,  
4  
5 respectively, indicating that CME is an important pathway for their uptake by DCs. To  
6  
7 confirm this, we tested a dynamin-inhibitor, dynasore, as dynamin is essential for  
8  
9 clathrin-coated vesicle formation<sup>65</sup>. Dynasore tends to interfere with the GTPase activity  
10  
11 of Dynamin and suppresses the pinching-off process but not the formation of clathrin-  
12  
13 coated pits in contrast to chlorpromazine<sup>66</sup>. Dynasore decreased the uptake of  
14  
15 AuZwTriMan and AuZw by 42% and 59%, respectively, confirming the importance of  
16  
17 clathrin in initiating endocytosis for both Au NCs.  
18  
19  
20

21  
22 EIPA, an inhibitor of macropinocytosis, reduced AuZwTriMan uptake by 47% and AuZw  
23  
24 by 21%. Macropinocytosis is a form of endocytosis that involves coordinated cytoskeletal  
25  
26 changes at the cell surface<sup>67</sup>. This result seems to suggest a less significant contribution  
27  
28 for macropinocytosis in NC processing than that reported in other studies, which have  
29  
30 ascribed macropinocytosis a major role in the engulfment of NPs by macrophages such as  
31  
32 DCs<sup>63</sup>. CytD is a drug that can depolymerise F-actin filaments and disrupt the  
33  
34 cytoskeleton. CytD has been reported to interfere with macropinocytosis and caveolae-  
35  
36 dependent uptake without affecting CME<sup>63</sup>. Treatment with CytD induced a strong 82%  
37  
38 decrease in AuZwTriMan uptake and a 43% decrease for AuZw. However, results from  
39  
40 CytD treatment need to be interpreted with caution as its action is extremely broad,  
41  
42 affecting all endocytic pathways and as well as many other biological processes<sup>68</sup>. Our  
43  
44 results suggest that the actin cytoskeleton plays a key role in Au NC endocytosis, which is  
45  
46 in agreement with the results of uptake mechanism studies performed on different types  
47  
48 of NP (QD<sup>69</sup>, polystyrene<sup>70</sup>, chitosan<sup>62</sup>) with sizes smaller than 50 nm in DCs. Our results  
49  
50 suggest that the endocytic uptake of AuZw by DCs occurs via multiple mechanisms with  
51  
52  
53  
54  
55  
56  
57  
58  
59  
60

1  
2  
3 major roles for clathrin and F-actin dependent endocytic pathways. Similar DC uptake  
4  
5 behaviour has been reported by Zhang and colleagues using carboxyl-coated Quantum  
6  
7 Dots ( $\text{\O} = 18 \text{ nm}$ )<sup>69</sup>.  
8  
9

10  
11  
12 Microtubules are a major class of cytoskeletal fibre, responsible for vesicular trafficking  
13  
14 among many other biological functions. The nocodazole inhibitor, which disrupts the  
15  
16 microtubule cytoskeleton, did not strongly affect the DC uptake of either type of Au NC  
17  
18 with an 11% decrease in both cases. This is consistent with a study performed by Dawson  
19  
20 et al. which showed that microtubule function was required for the uptake of larger (200  
21  
22 nm) but not smaller (40 nm) NPs<sup>70</sup>.  
23  
24  
25  
26  
27

## 28 **CONCLUSIONS**

29  
30  
31 In summary, Au NCs stabilised by a mixture of zwitterionic and trivalent mannose  
32  
33 ligands were prepared using the crystal growth/reduction method. Chemical and optical  
34  
35 characterisation confirmed their ultra-small size ( $\text{\O} \sim 2 \text{ nm}$ ), fluorescence emission in the  
36  
37 red-NIR window and the activity of their carbohydrate ligands. Interestingly, an  
38  
39 aggregation induced emission (AIE) enhancement was observed for Au NCs coated with  
40  
41 the mannose ligand in the presence of the lectin ConA. Measurements of Au NCs  
42  
43 dispersed in complete medium showed relatively high colloidal and fluorescence stability.  
44  
45  
46 Studies in DCs showed a greater than 2.5 fold increase in particle uptake when stabilised  
47  
48 by a trivalent mannose ligand versus a zwitterionic ligand alone. Experiments using  
49  
50 inhibitors that target different uptake mechanisms suggest that DCs uptake Au NCs via  
51  
52 multiple endocytic pathways with major roles for clathrin-mediated and F-actin  
53  
54 dependent mechanisms. The 60% reduction in the uptake of mannose-coated Au NCs by  
55  
56  
57  
58  
59  
60

1  
2  
3 the presence of a C-lectin inhibitor clearly demonstrates the specific targeting of Au NCs  
4  
5 to DCs via C-lectin receptors. Electron microscopy data supports the hypothesis that Au  
6  
7 NCs are engulfed by endocytosis, with particles present in both endosomes and  
8  
9 lysosomes.  
10

11  
12 Regarding future applications, carbohydrate-ligand stabilized gold nanoclusters have  
13  
14 great potential as a delivery system due to their low cytotoxicity, good colloidal stability,  
15  
16 and strong uptake in DCs at very low concentrations ( $1 \mu\text{g}\cdot\text{mL}^{-1}$ ) thanks to their  
17  
18 interaction with C-lectin receptors on the DC surface and their ultra-small size (i.e. high  
19  
20 diffusion). The original optical properties of NCs allow them to be visualised by  
21  
22 fluorescence in the red-NIR window and potentially by other techniques such as X-ray  
23  
24 tomography or photoacoustic imaging, as well as exploited for their photothermal  
25  
26 properties due to their gold nature.  
27  
28  
29  
30  
31  
32  
33

34 **Supporting information.** Ligand synthesis & characterisation; additional chemical and  
35  
36 optical characterisation of NCs, cell studies including cytotoxicity and inhibitory  
37  
38 experiments are supplied as Supporting Information.  
39  
40  
41  
42

#### 43 **Acknowledgements**

44  
45  
46  
47 This work was supported by the Instituto de Salud Carlos III (ISCII) (project N°  
48  
49 CP12/03310), by the Ministerio de Economía y Competitividad (MINECO) (CTQ2011-  
50  
51 23410), co-financed by European Regional Development Fund (ERDF) and by ISCIII-  
52  
53 Thematic Networks and Co-operative Research Centers: RIRAAF (RD012/0013), Junta  
54  
55 de Andalucía (CTS-7433), and ISCIII (PI12/02481-PI/02529). Xavier Le Guevel would  
56  
57  
58  
59  
60

1  
2  
3 like to thank Daniel Sierra for the zwitterion ligand synthesis, Carlos Rodriguez for the  
4  
5 mass spectrometry analysis, José Maria Montenegro for the fluorescence lifetime  
6  
7 measurement, Juan Felix Lopez (BIONAND Nanoimaging Unit) for the TEM  
8  
9 measurements and John Pearson (BIONAND Nanoimaging Unit) for the optical  
10  
11 microscopy analysis and critical reading of the manuscript.  
12  
13  
14  
15  
16  
17  
18  
19

## 20 REFERENCES

- 21  
22  
23 1. Cruz, L. J.; Tacke, P. J.; Fokkink, R.; Joosten, B.; Stuart, M. C.; Albericio, F.;  
24 Torensma, R.; Figdor, C. G., Targeted PLGA nano- but not microparticles specifically  
25 deliver antigen to human dendritic cells via DC-SIGN in vitro. *Journal of Controlled*  
26 *Release* **2010**, *144* (2), 118-126.  
27 2. Marradi, M.; Chiodo, F.; García, I.; Penadés, S., Glyconanoparticles as multifunctional  
28 and multimodal carbohydrate systems. *Chemical Society Reviews* **2013**, *42* (11), 4728-  
29 4745.  
30 3. Novak, N., Targeting Dendritic Cells in Allergen Immunotherapy. *Immunology and*  
31 *Allergy Clinics of North America* **2006**, *26* (2), 307-319.  
32 4. Abbas, A. K.; Sharpe, A. H., Dendritic cells give and take away. *Nature*  
33 *Immunology* **2005**, *6* (3), 227-228.  
34 5. Mellman, I.; Steinman, R. M., Dendritic cells: Specialized and regulated antigen  
35 processing machines. *Cell* **2001**, *106* (3), 255-258.  
36 6. Hubbell, J. A.; Thomas, S. N.; Swartz, M. A., Materials engineering for  
37 immunomodulation. *Nature* **2009**, *462* (7272), 449-460.  
38 7. Kim, J.; Mooney, D. J., In vivo modulation of dendritic cells by engineered materials:  
39 Towards new cancer vaccines. *Nano Today* **2011**, *6* (5), 466-477.  
40 8. Kreutz, M.; Tacke, P. J.; Figdor, C. G., Targeting dendritic cells--why bother? *Blood*  
41 **2013**, *121* (15), 2836-2844.  
42 9. Dobrovolskaia, M. A.; McNeil, S. E., Immunological properties of engineered  
43 nanomaterials. *Nature Nanotechnology* **2007**, *2* (8), 469-478.  
44 10. Klippstein, R.; Pozo, D., Nanotechnology-based manipulation of dendritic cells for  
45 enhanced immunotherapy strategies. *Nanomedicine: Nanotechnology, Biology, and*  
46 *Medicine* **2010**, *6* (4), 523-529.  
47 11. Reddy, S. T.; Rehor, A.; Schmoekel, H. G.; Hubbell, J. A.; Swartz, M. A., In vivo  
48 targeting of dendritic cells in lymph nodes with poly(propylene sulfide) nanoparticles.  
49 *Journal of Controlled Release* **2006**, *112* (1), 26-34.  
50 12. Hirosue, S.; Kourtis, I. C.; van der Vlies, A. J.; Hubbell, J. A.; Swartz, M. A.,  
51 Antigen delivery to dendritic cells by poly(propylene sulfide) nanoparticles with disulfide  
52  
53  
54  
55  
56  
57  
58  
59  
60



1  
2  
3 conjugated peptides: Cross-presentation and T cell activation. *Vaccine* **2010**, *28* (50),  
4 7897-7906.

5  
6 13. García-Vallejo, J. J.; Ambrosini, M.; Overbeek, A.; van Riel, W. E.; Bloem, K.;  
7 Unger, W. W. J.; Chiodo, F.; Bolscher, J. G.; Nazmi, K.; Kalay, H.; van Kooyk, Y.,  
8 Multivalent glycopeptide dendrimers for the targeted delivery of antigens to dendritic  
9 cells. *Molecular Immunology* **2013**, *53* (4), 387-397.

10  
11 14. Moffat, J. M.; Cheong, W. S.; Villadangos, J. A.; Mintern, J. D.; Netter, H. J.,  
12 Hepatitis B virus-like particles access major histocompatibility class I and II antigen  
13 presentation pathways in primary dendritic cells. *Vaccine* **2013**, *31* (18), 2310-2316.

14  
15 15. Unger, W. W. J.; Van Beelen, A. J.; Bruijns, S. C.; Joshi, M.; Fehres, C. M.; Van  
16 Bloois, L.; Verstege, M. I.; Ambrosini, M.; Kalay, H.; Nazmi, K.; Bolscher, J. G.;  
17 Hooijberg, E.; De Gruijl, T. D.; Storm, G.; Van Kooyk, Y., Glycan-modified liposomes  
18 boost CD4 + and CD8 + T-cell responses by targeting DC-SIGN on dendritic cells.  
19 *Journal of Controlled Release* **2012**, *160* (1), 88-95.

20  
21 16. Chiodo, F.; Marradi, M.; Park, J.; Ram, A. F. J.; Penadés, S.; Van Die, I.; Tefsen,  
22 B., Galactofuranose-coated gold nanoparticles elicit a pro-inflammatory response in  
23 human monocyte-derived dendritic cells and are recognized by DC-SIGN. *ACS Chemical*  
24 *Biology* **2014**, *9* (2), 383-389.

25  
26 17. Shahbazi, M. A.; Fernández, T. D.; Mäkilä, E. M.; Le Guével, X.; Mayorga, C.;  
27 Kaasalainen, M. H.; Salonen, J. J.; Hirvonen, J. T.; Santos, H. A., Surface chemistry  
28 dependent immunostimulative potential of porous silicon nanoplatfoms. *Biomaterials*  
29 **2014**, *35* (33), 9224-9235.

30  
31 18. Tomić, S.; Dokić, J.; Vasilijić, S.; Ogrinc, N.; Rudolf, R.; Pelicon, P.; Vučević, D.;  
32 Milosavljević, P.; Janković, S.; Anžel, I.; Rajković, J.; Rupnik, M. S.; Friedrich, B.;  
33 Čolić, M., Size-dependent effects of gold nanoparticles uptake on maturation and  
34 antitumor functions of human dendritic cells in vitro. *PLoS ONE* **2014**, *9* (5).

35  
36 19. Reddy, S. T.; Van Der Vlies, A. J.; Simeoni, E.; Angeli, V.; Randolph, G. J.;  
37 O'Neil, C. P.; Lee, L. K.; Swartz, M. A.; Hubbell, J. A., Exploiting lymphatic transport  
38 and complement activation in nanoparticle vaccines. *Nature Biotechnology* **2007**, *25* (10),  
39 1159-1164.

40  
41 20. Huo, S.; Ma, H.; Huang, K.; Liu, J.; Wei, T.; Jin, S.; Zhang, J.; He, S.; Liang, X. J.,  
42 Superior penetration and retention behavior of 50 nm gold nanoparticles in tumors.  
43 *Cancer Research* **2013**, *73* (1), 319-330.

44  
45 21. Hirsjärvi, S.; Dufort, S.; Gravier, J.; Texier, I.; Yan, Q.; Bibette, J.; Sancey, L.;  
46 Josserand, V.; Passirani, C.; Benoit, J. P.; Coll, J. L., Influence of size, surface coating  
47 and fine chemical composition on the in vitro reactivity and in vivo biodistribution of  
48 lipid nanocapsules versus lipid nanoemulsions in cancer models. *Nanomedicine:*  
49 *Nanotechnology, Biology, and Medicine* **2013**, *9* (3), 375-387.

50  
51 22. Moros, M.; Hernández, B.; Garet, E.; Dias, J. T.; Sáez, B.; Grazú, V.; González-  
52 Fernández, A.; Alonso, C.; De La Fuente, J. M., Monosaccharides versus PEG-  
53 functionalized NPs: Influence in the cellular uptake. *ACS Nano* **2012**, *6* (2), 1565-1577.

54  
55 23. Figdor, C. G.; Van Kooyk, Y.; Adema, G. J., C-type lectin receptors on dendritic  
56 cells and langerhans cells. *Nature Reviews Immunology* **2002**, *2* (2), 77-84.

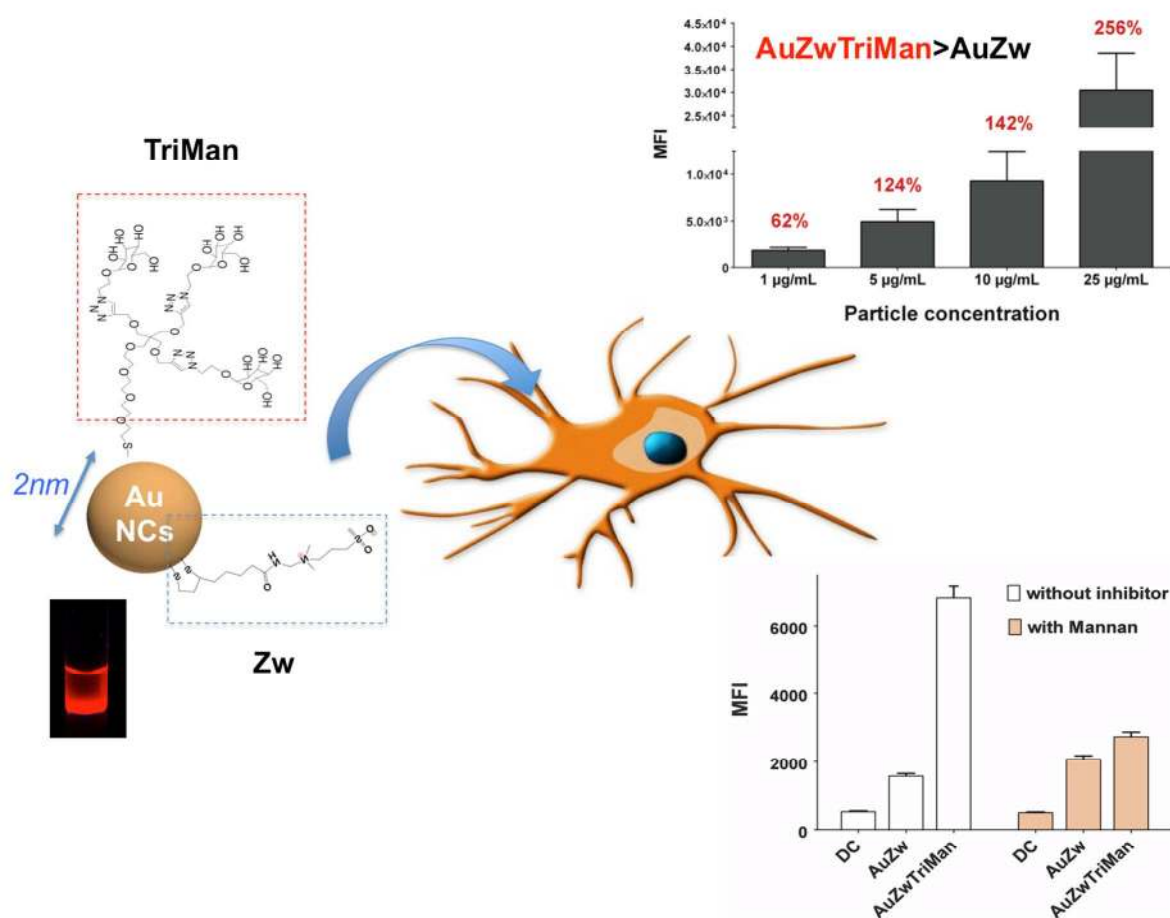
57  
58 24. Bernardi, A.; Jiménez-Barbero, J.; Casnati, A.; De Castro, C.; Darbre, T.; Fieschi,  
59 F.; Finne, J.; Funken, H.; Jaeger, K. E.; Lahmann, M.; Lindhorst, T. K.; Marradi, M.;  
60 Messner, P.; Molinaro, A.; Murphy, P. V.; Nativi, C.; Oscarson, S.; Penadés, S.; Peri, F.;

- Pieters, R. J.; Renaudet, O.; Reymond, J. L.; Richichi, B.; Rojo, J.; Sansone, F.; Schäffer, C.; Turnbull, W. B.; Velasco-Torrijos, T.; Vidal, S.; Vincent, S.; Wennekes, T.; Zuilhof, H.; Imberty, A., Multivalent glycoconjugates as anti-pathogenic agents. *Chemical Society Reviews* **2013**, *42* (11), 4709-4727.
25. Ribeiro-Viana, R.; García-Vallejo, J. J.; Collado, D.; Pérez-Inestrosa, E.; Bloem, K.; Van Kooyk, Y.; Rojo, J., BODIPY-labeled DC-SIGN-targeting glycodendrons efficiently internalize and route to lysosomes in human dendritic cells. *Biomacromolecules* **2012**, *13* (10), 3209-3219.
26. Luczkowiak, J.; Muñoz, A.; Sánchez-Navarro, M.; Ribeiro-Viana, R.; Ginieis, A.; Illescas, B. M.; Martín, N.; Delgado, R.; Rojo, J., Glycofullerenes inhibit viral infection. *Biomacromolecules* **2013**, *14* (2), 431-437.
27. Sattin, S.; Daghett, A.; Thépaut, M.; Berzi, A.; Sánchez-Navarro, M.; Tabarani, G.; Rojo, J.; Fieschi, F.; Clerici, M.; Bernardi, A., Inhibition of DC-SIGN-mediated HIV infection by a linear trimannoside mimic in a tetravalent presentation. *ACS Chemical Biology* **2010**, *5* (3), 301-312.
28. Luczkowiak, J.; Sattin, S.; Sutkevičiute, I.; Reina, J. J.; Sánchez-Navarro, M.; Thépaut, M.; Martínez-Prats, L.; Daghetti, A.; Fieschi, F.; Delgado, R.; Bernardi, A.; Rojo, J., Pseudosaccharide functionalized dendrimers as potent inhibitors of DC-SIGN dependent ebola pseudotyped viral infection. *Bioconjugate Chemistry* **2011**, *22* (7), 1354-1365.
29. Ribeiro-Viana, R.; Sánchez-Navarro, M.; Luczkowiak, J.; Koeppe, J. R.; Delgado, R.; Rojo, J.; Davis, B. G., Virus-like glycodendrinanoparticles displaying quasi-equivalent nested polyvalency upon glycoprotein platforms potently block viral infection. *Nature Communications* **2012**, *3*, 1-8.
30. Jin, R., Quantum sized, thiolate-protected gold nanoclusters. *Nanoscale* **2010**, *2* (3), 343-362.
31. Zheng, J.; Zhou, C.; Yu, M.; Liu, J., Different sized luminescent gold nanoparticles. *Nanoscale* **2012**, *4* (14), 4073-4083.
32. Zheng, J.; Nicovich, P. R.; Dickson, R. M., Highly fluorescent noble-metal quantum dots. *Annual Review of Physical Chemistry* **2007**, *58*, 409-431.
33. Goswami, N.; Zheng, K.; Xie, J., Bio-NCs-the marriage of ultrasmall metal nanoclusters with biomolecules. *Nanoscale* **2014**, *6* (22), 13328-13347.
34. Jiang, D. E., The expanding universe of thiolated gold nanoclusters and beyond. *Nanoscale* **2013**, *5* (16), 7149-7160.
35. Zhu, M.; Aikens, C. M.; Hollander, F. J.; Schatz, G. C.; Jin, R., Correlating the crystal structure of A thiol-protected Au<sub>25</sub> cluster and optical properties. *Journal of the American Chemical Society* **2008**, *130* (18), 5883-5885.
36. Le Guével, X.; Tagit, O.; Rodríguez, C. E.; Trouillet, V.; Pernia Leal, M.; Hildebrandt, N., Ligand effect on the size, valence state and red/near infrared photoluminescence of bidentate thiol gold nanoclusters. *Nanoscale* **2014**, *6* (14), 8091-8099.
37. Negishi, Y.; Nobusada, K.; Tsukuda, T., Glutathione-protected gold clusters revisited: Bridging the gap between gold(I)-thiolate complexes and thiolate-protected gold nanocrystals. *Journal of the American Chemical Society* **2005**, *127* (14), 5261-5270.
38. Wang, G.; Guo, R.; Kalyuzhny, G.; Choi, J. P.; Murray, R. W., NIR luminescence intensities increase linearly with proportion of polar thiolate ligands in protecting

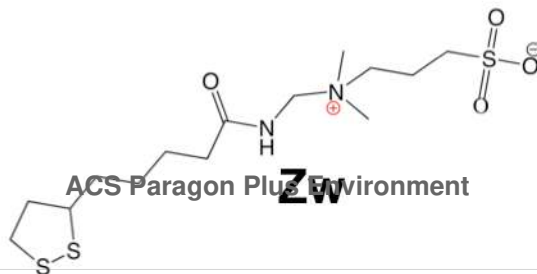
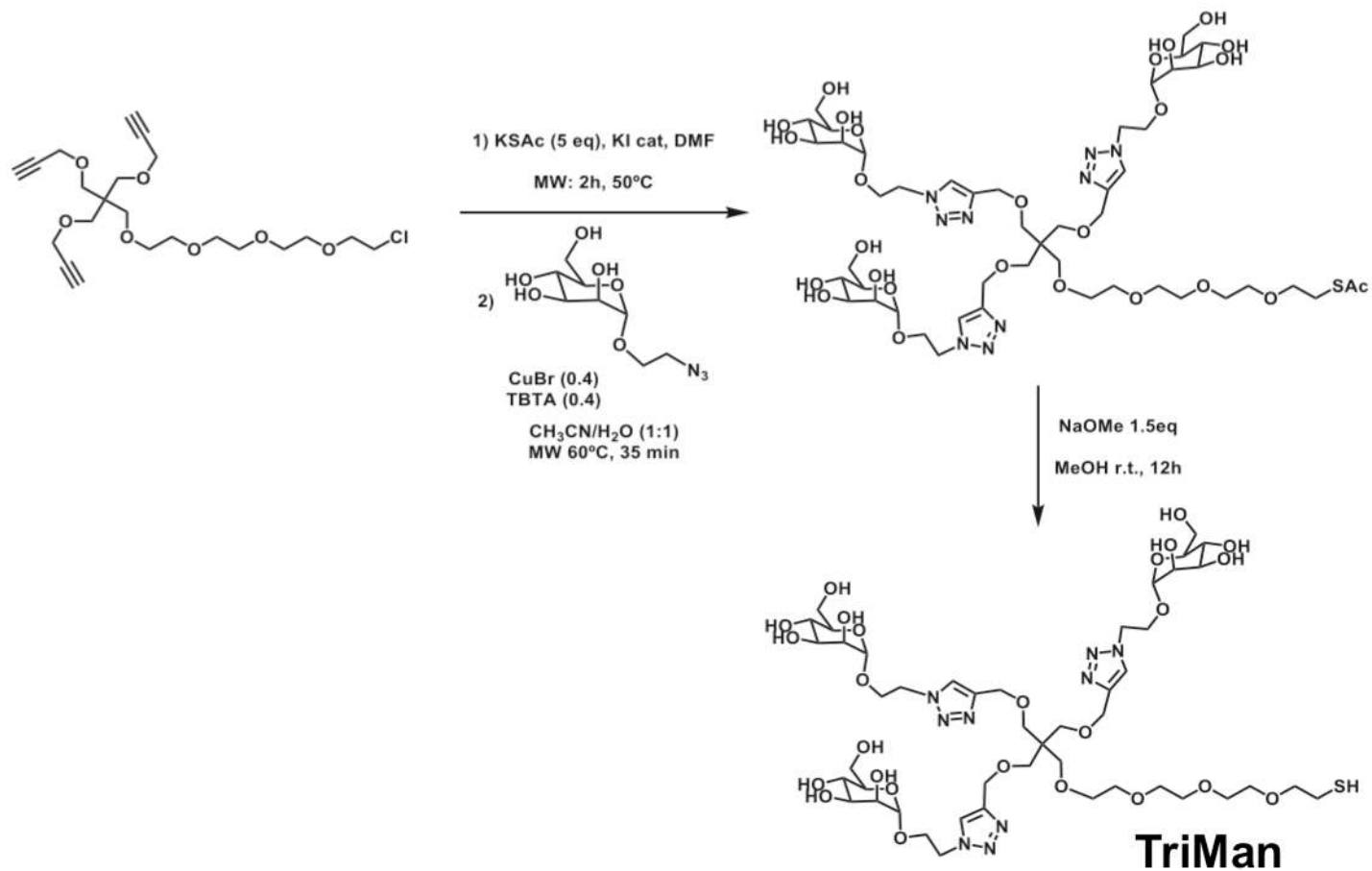
- 1  
2  
3 monolayers of Au 38 and Au 140 quantum dots. *Journal of Physical Chemistry B* **2006**,  
4 *110* (41), 20282-20289.
- 5  
6 39. Yu, Y.; Luo, Z.; Chevrier, D. M.; Leong, D. T.; Zhang, P.; Jiang, D. E.; Xie, J.,  
7 Identification of a highly luminescent Au<sub>22</sub>(SG)<sub>18</sub> nanocluster. *Journal of the American*  
8 *Chemical Society* **2014**, *136* (4), 1246-1249.
- 9  
10 40. Aldeek, F.; Muhammed, M. A. H.; Palui, G.; Zhan, N.; Mattoussi, H., Growth of  
11 highly fluorescent polyethylene glycol- and zwitterion- functionalized gold nanoclusters.  
12 *ACS Nano* **2013**, *7* (3), 2509-2521.
- 13  
14 41. Le Guével, X.; Spies, C.; Daum, N.; Jung, G.; Schneider, M., Highly fluorescent  
15 silver nanoclusters stabilized by glutathione: A promising fluorescent label for  
16 bioimaging. *Nano Research* **2012**, *5* (6), 379-387.
- 17  
18 42. Muhammed, M. A. H.; Ramesh, S.; Sinha, S. S.; Pal, S. K.; Pradeep, T., Two  
19 Distinct Fluorescent Quantum Clusters of Gold Starting from Metallic Nanoparticles by  
20 pH-Dependent Ligand Etching. *Nanoresearch* **2008**, *1*, 333-340.
- 21  
22 43. Le Guével, X.; Hötzer, B.; Jung, G.; Hollemeyer, K.; Trouillet, V.; Schneider, M.,  
23 Formation of fluorescent metal (Au, Ag) nanoclusters capped in bovine serum albumin  
24 followed by fluorescence and spectroscopy. *Journal of Physical Chemistry C* **2011**, *115*  
25 (22), 10955-10963.
- 26  
27 44. Shang, L.; Azadfar, N.; Stockmar, F.; Send, W.; Trouillet, V.; Bruns, M.;  
28 Gerthsen, D.; Nienhaus, G. U., One-pot synthesis of near-infrared fluorescent gold  
29 clusters for cellular fluorescence lifetime imaging. *Small* **2011**, *7* (18), 2614-2620.
- 30  
31 45. Luo, Z.; Yuan, X.; Yu, Y.; Zhang, Q.; Leong, D. T.; Lee, J. Y.; Xie, J., From  
32 aggregation-induced emission of Au(I)-thiolate complexes to ultrabright Au(0)@Au(I)-  
33 thiolate core-shell nanoclusters. *Journal of the American Chemical Society* **2012**, *134*  
34 (40), 16662-16670.
- 35  
36 46. Chan, P. H.; Ghosh, B.; Lai, H. Z.; Peng, H. L.; Mong, K. K. T.; Chen, Y. C.,  
37 Photoluminescent Gold Nanoclusters as Sensing Probes for Uropathogenic *Escherichia*  
38 *coli*. *PLoS ONE* **2013**, *8* (3).
- 39  
40 47. Wang, H. H.; Lin, C. A. J.; Lee, C. H.; Lin, Y. C.; Tseng, Y. M.; Hsieh, C. L.;  
41 Chen, C. H.; Tsai, C. H.; Hsieh, C. T.; Shen, J. L.; Chan, W. H.; Chang, W. H.; Yeh, H.  
42 I., Fluorescent gold nanoclusters as a biocompatible marker for in vitro and in vivo  
43 tracking of endothelial cells. *ACS Nano* **2011**, *5* (6), 4337-4344.
- 44  
45 48. Kunwar, P.; Hassinen, J.; Bautista, G.; Ras, R. H. A.; Toivonen, J., Direct laser  
46 writing of photostable fluorescent silver nanoclusters in polymer films. *ACS Nano* **2014**, *8*  
47 (11), 11165-11171.
- 48  
49 49. Liu, J.; Yu, M.; Zhou, C.; Yang, S.; Ning, X.; Zheng, J., Passive tumor targeting of  
50 renal-clearable luminescent gold nanoparticles: Long tumor retention and fast normal  
51 tissue clearance. *Journal of the American Chemical Society* **2013**, *135* (13), 4978-4981.
- 52  
53 50. Zhou, C.; Long, M.; Qin, Y.; Sun, X.; Zheng, J., Luminescent gold nanoparticles  
54 with efficient renal clearance. *Angewandte Chemie - International Edition* **2011**, *50* (14),  
55 3168-3172.
- 56  
57 51. Zhang, X. D.; Chen, J.; Luo, Z.; Wu, D.; Shen, X.; Song, S. S.; Sun, Y. M.; Liu, P.  
58 X.; Zhao, J.; Huo, S.; Fan, S.; Fan, F.; Liang, X. J.; Xie, J., Enhanced tumor accumulation  
59 of Sub-2 nm gold nanoclusters for cancer radiation therapy. *Advanced Healthcare*  
60 *Materials* **2014**, *3* (1), 133-141.

- 1  
2  
3  
4  
5  
6  
7  
8  
9  
10  
11  
12  
13  
14  
15  
16  
17  
18  
19  
20  
21  
22  
23  
24  
25  
26  
27  
28  
29  
30  
31  
32  
33  
34  
35  
36  
37  
38  
39  
40  
41  
42  
43  
44  
45  
46  
47  
48  
49  
50  
51  
52  
53  
54  
55  
56  
57  
58  
59  
60
52. Fernandez, T. D.; Pearson, J. R.; Pernia Leal, M.; Torres, M. J.; Blanca, M.; Mayorga, C.; Le Guével, X., Intracellular accumulation and immunological properties of fluorescent gold nanoclusters in human dendritic cells. *Biomaterials* **2015**, *43*, 1-12.
53. Park, J.; Nam, J.; Won, N.; Jin, H.; Jung, S.; Jung, S.; Cho, S. H.; Kim, S., Compact and stable quantum dots with positive, negative, or zwitterionic surface: Specific cell interactions and non-specific adsorptions by the surface charges. *Advanced Functional Materials* **2011**, *21* (9), 1558-1566.
54. Dou, X.; Yuan, X.; Yao, Q.; Luo, Z.; Zheng, K.; Xie, J., Facile synthesis of water-soluble Au<sub>25</sub>Ag<sub>x</sub> nanoclusters protected by mono- and bi-thiolate ligands. *Chemical Communications* **2014**, *50* (56), 7459-7462.
55. Wu, Z.; Jin, R., On the ligand's role in the fluorescence of gold nanoclusters. *Nano Letters* **2010**, *10* (7), 2568-2573.
56. Le Guevel, X., Recent advances on the synthesis of metal quantum nanoclusters and their application for bioimaging. *IEEE Journal on Selected Topics in Quantum Electronics* **2014**, *20* (3), 1-12.
57. Zhou, C.; Sun, C.; Yu, M.; Qin, Y.; Wang, J.; Kim, M.; Zheng, J., Luminescent gold nanoparticles with mixed valence states generated from dissociation of polymeric Au(I) thiolates. *Journal of Physical Chemistry C* **2010**, *114* (17), 7727-7732.
58. Hong, Y.; Lam, J. W. Y.; Tang, B. Z., Aggregation-induced emission. *Chemical Society Reviews* **2011**, *40* (11), 5361-5388.
59. Jia, X.; Li, J.; Wang, E., Cu Nanoclusters with Aggregation Induced Emission Enhancement. *small* **2013**, *9* (22), 3873-3879.
60. Dunn, K. W.; Kamocka, M. M.; McDonald, J. H., A practical guide to evaluating colocalization in biological microscopy. *American Journal of Physiology - Cell Physiology* **2011**, *300* (4), C723-C742.
61. Engering, A. J.; Cella, M.; Fluitsma, D.; Brockhaus, M.; Hoefsmit, E. C. M.; Lanzavecchia, A.; Pieters, J., The mannose receptor functions as a high capacity and broad specificity antigen receptor in human dendritic cells. *European Journal of Immunology* **1997**, *27* (9), 2417-2425.
62. Nam, H. Y.; Kwon, S. M.; Chung, H.; Lee, S. Y.; Kwon, S. H.; Jeon, H.; Kim, Y.; Park, J. H.; Kim, J.; Her, S.; Oh, Y. K.; Kwon, I. C.; Kim, K.; Jeong, S. Y., Cellular uptake mechanism and intracellular fate of hydrophobically modified glycol chitosan nanoparticles. *Journal of Controlled Release* **2009**, *135* (3), 259-267.
63. Khalil, I. A.; Kogure, K.; Akita, H.; Harashima, H., Uptake pathways and subsequent intracellular trafficking in nonviral gene delivery. *Pharmacological Reviews* **2006**, *58* (1), 32-45.
64. Chen, C. L.; Hou, W. H.; Liu, I. H.; Hsiao, G.; Huang, S. S.; Huang, J. S., Inhibitors of clathrin-dependent endocytosis enhance TGF $\beta$  signaling and responses. *J. Cell Sci.* **2009**, *122* (11), 1863-1871.
65. Macia, E.; Ehrlich, M.; Massol, R.; Boucrot, E.; Brunner, C.; Kirchhausen, T., Dynasore, a Cell-Permeable Inhibitor of Dynamin. *Dev. Cell* **2006**, *10* (6), 839-850.
66. Shang, L.; Nienhaus, K.; Jiang, X.; Yang, L.; Landfester, K.; Mailänder, V.; Simmet, T.; Nienhaus, G., Nanoparticle interactions with live cells: Quantitative fluorescence microscopy of nanoparticle size effects. *Belstein Journal of Nanotechnology* **2014**, *5*, 2388-2397.

67. Falcone, S.; Cocucci, E.; Podini, P.; Kirchhausen, T.; Clementi, E.; Meldolesi, J., Macropinocytosis: Regulated coordination of endocytic and exocytic membrane traffic events. *J. Cell Sci.* **2006**, *119* (22), 4758-4769.
68. Zegers, M. M. P.; Zaal, K. J. M.; Van Ijzendoorn, S. C. D.; Klappe, K.; Hoekstra, D., Actin filaments and microtubules are involved in different membrane traffic pathways that transport sphingolipids to the apical surface of polarized HepG2 cells. *Mol. Biol. Cell* **1998**, *9* (7), 1939-1949.
69. Zhang, L. W.; Bäumer, W.; Monteiro-Riviere, N. A., Cellular uptake mechanisms and toxicity of quantum dots in dendritic cells. *Nanomedicine* **2011**, *6* (5), 777-791.
70. dos Santos, T.; Varela, J.; Lynch, I.; Salvati, A.; Dawson, K. A., Effects of transport inhibitors on the cellular uptake of carboxylated polystyrene nanoparticles in different cell lines. *PLoS ONE* **2011**, *6* (9).



Fluorescent gold nanoclusters (size ≈ 2 nm) are readily taken up by human dendritic cells via endocytic mechanisms when stabilized by a mixture of zwitterionic and multivalent mannose ligands. This strong uptake depends specifically on interactions between the coated nanoclusters and cellular C-lectin mannose receptors.



	Wt.% organic moiety*	Wt. % of Man**	<u>Au:S</u> ***	Molecular weight****
--	----------------------	----------------	-----------------	----------------------

1  
2  
3  
4  
5  
6 AuZw

80±3

0

1:8.9

~14kDa

7  
8  
9 AuZwTriMan

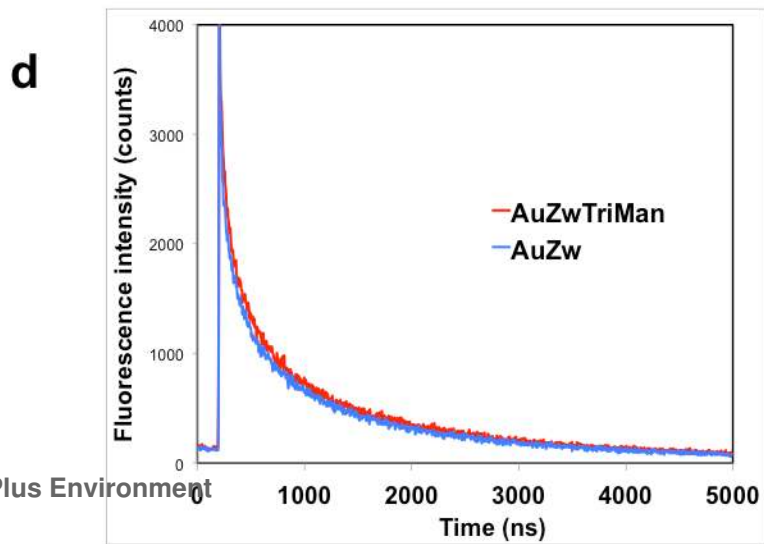
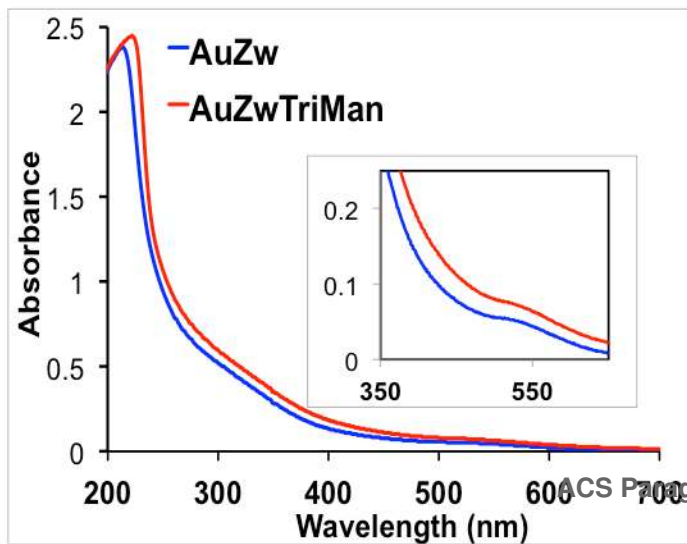
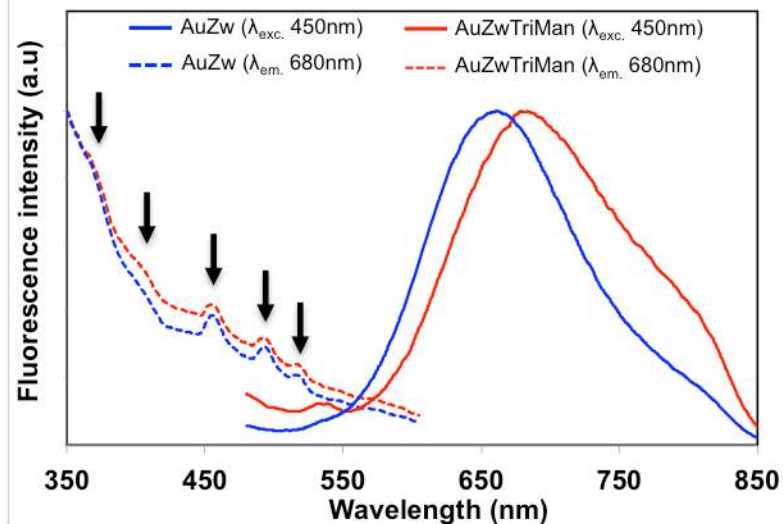
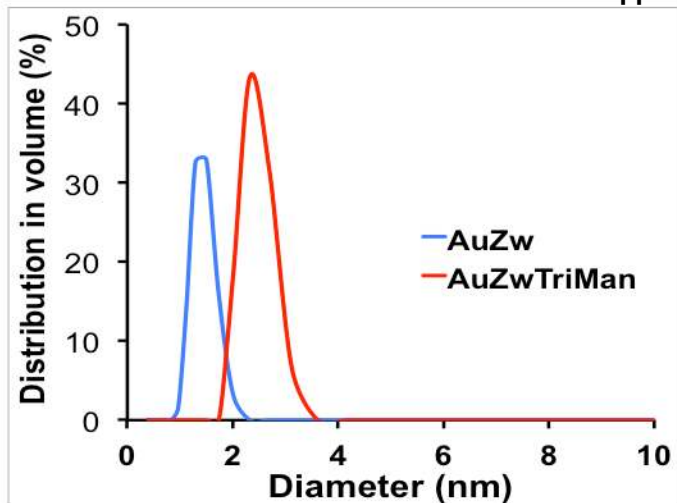
83±3

8±2

1:12.5

~17kDa

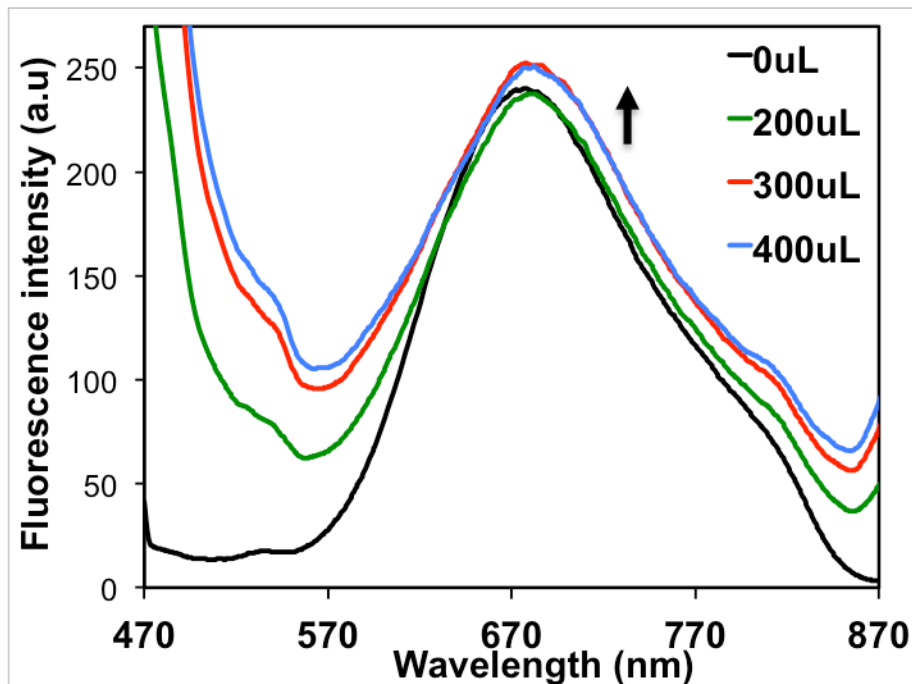
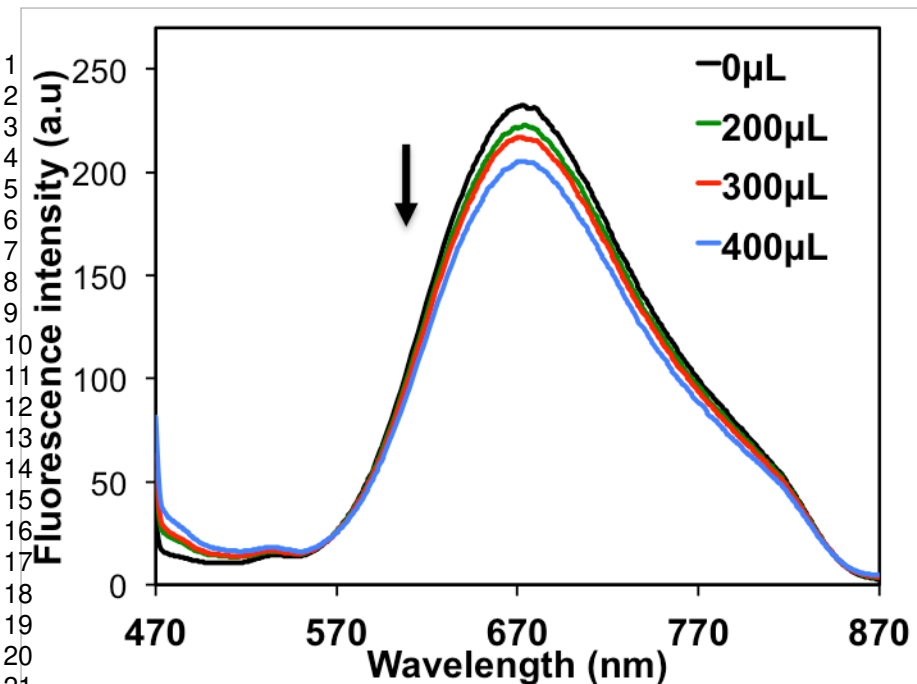
10  
11  
12  
13  
14  
15  
16 \*: determined by thermogravimetry; \*\*: determined by anthrone test; \*\*\*: measurements  
17 performed by ICP; \*\*\*\*: Value estimated for the fluorescent Au NCs by MALDI/Tof  
18  
19  
20 analyses.  
21  
22  
23  
24  
25



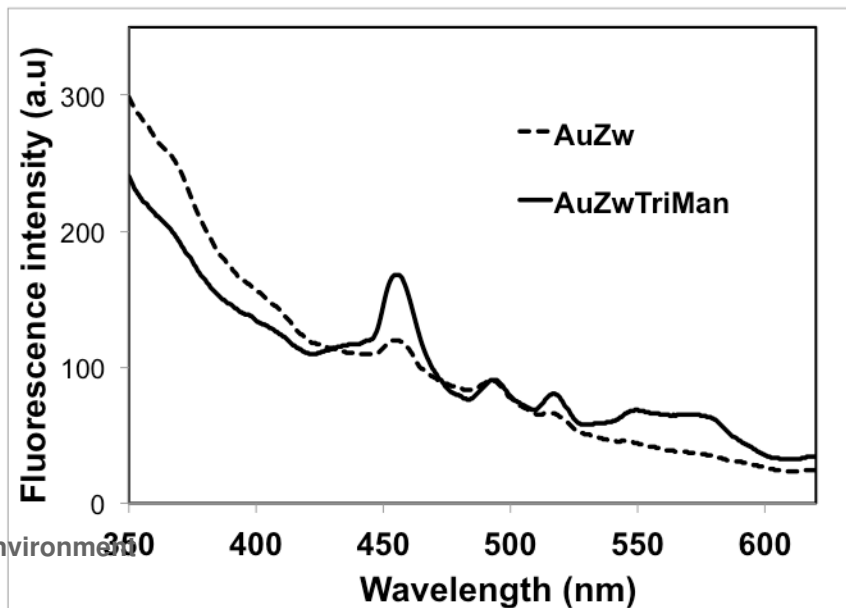


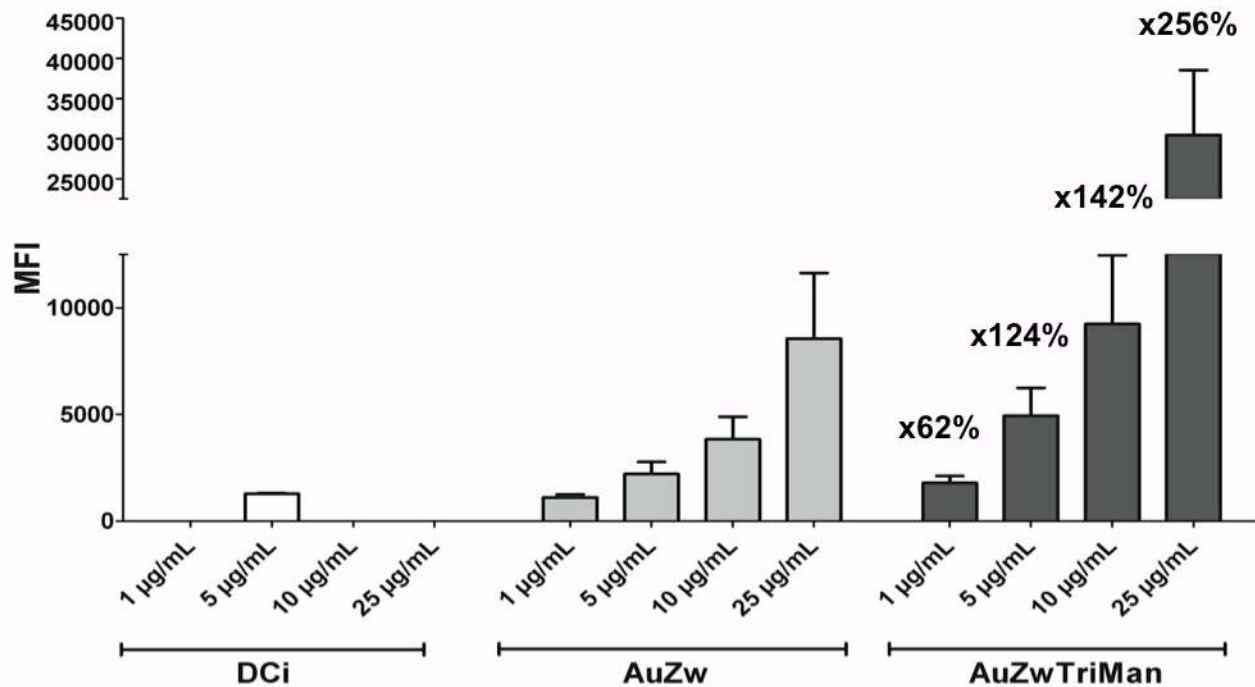
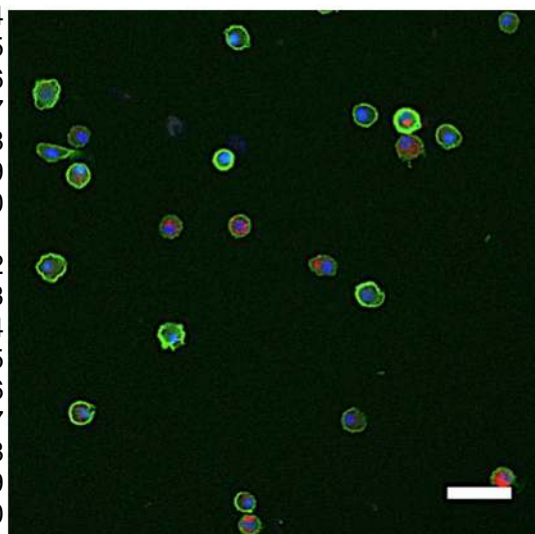
	$\lambda_{\text{em.}}$ *	Relative fluorescence intensity**		Lifetime		$\phi$ ***
		Water	PBS (10mM, pH 7.2)	Water	PBS (10mM, pH 7.2)	
<u><i>AuZw</i></u>	665nm	1	0.97	$\tau_1=1.53\mu\text{s}$ (85%); $\tau_2=312\text{ns}$ (15%)	$\tau_1=1.93\mu\text{s}$ (73%); $\tau_2=529\text{ns}$ (27%)	11.3
<u><i>AuZwTriMan</i></u>	680nm	0.89	0.79	$\tau_1=1.50\mu\text{s}$ (85%); $\tau_2=300\text{ns}$ (15%)	$\tau_1=1.90\mu\text{s}$ (69%); $\tau_2=541\text{ns}$ (27%)	8.7

\*  $\lambda_{\text{exc.}}=450\text{nm}$ ; \*\*: normalised to *AuZw* fluorescence intensity. Both NCs have absorbance at 0.1 using  $\lambda_{\text{exc.}}=450\text{nm}$ ; \*\*\* determined by comparison with Fluorescein ( $\phi=0.79$  in 0.1M NaOH).

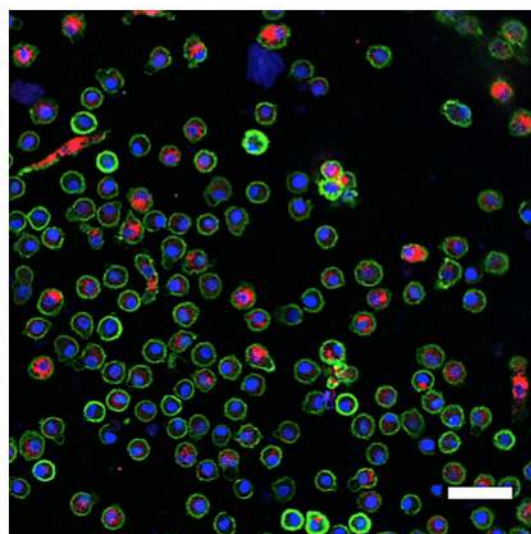
**c**

	<i>AuZw</i>			<i>AuZwTriMan</i>		
ConA (5mg.mL <sup>-1</sup> )	0 $\mu$ L	50 $\mu$ L	100 $\mu$ L	0 $\mu$ L	50 $\mu$ L	100 $\mu$ L
$\tau_1$	529ns (27%)	512ns (26%)	518ns (25%)	565ns (31%)	541ns (27%)	378ns (18%)
$\tau_2$	1.93 $\mu$ s (73%)	1.92 $\mu$ s (74%)	1.88 $\mu$ s (75%)	1.90 $\mu$ s (69%)	1.78 $\mu$ s (73%)	1.51 $\mu$ s (82%)
$\chi$	1.067	1.091	0.936	1.120	1.200	1.141

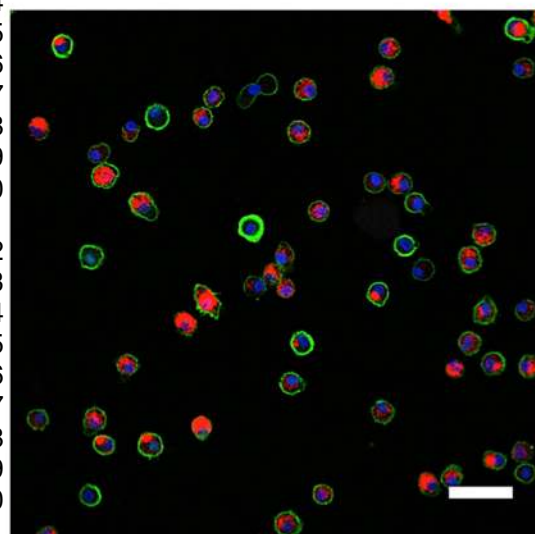
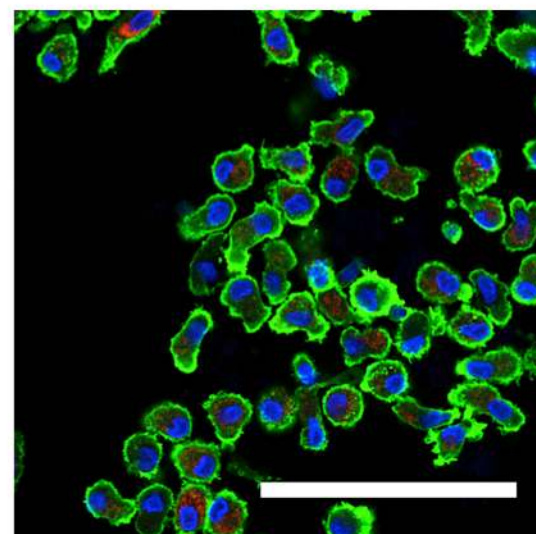
**d**

**b**

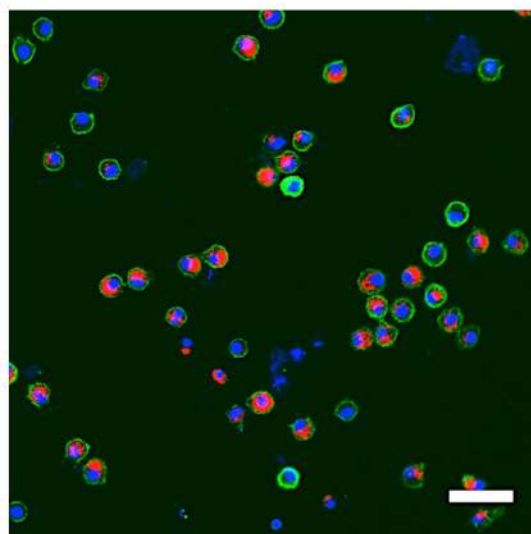
AuZw-5



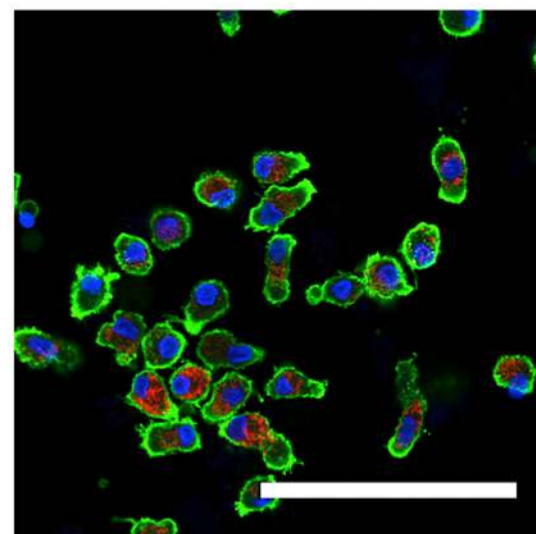
AuZw-10



AuZwTriMan-5



ACS Paragon Plus Environment



AuZwTriMan-10

